// Copyright Warning & Restrictions

The copyright law of the United States (Title 17, United States Code) governs the making of photocopies or other reproductions of copyrighted material.

Under certain conditions specified in the law, libraries and archives are authorized to furnish a photocopy or other reproduction. One of these specified conditions is that the photocopy or reproduction is not to be "used for any purpose other than private study, scholarship, or research." If a, user makes a request for, or later uses, a photocopy or reproduction for purposes in excess of "fair use" that user may be liable for copyright infringement,

This institution reserves the right to refuse to accept a copying order if, in its judgment, fulfillment of the order would involve violation of copyright law.

Please Note: The author retains the copyright while the New Jersey Institute of Technology reserves the right to distribute this thesis or dissertation

Printing note: If you do not wish to print this page, then select "Pages from: first page # to: last page #" on the print dialog screen

NJIT
New Jersey's Science & Technology University

The Van Houten library has removed some of the personal information and all signatures from the approval page and biographical sketches of theses and dissertations in order to protect the identity of NJIT graduates and faculty.

# ABSTRACT

## LASER ABLATION OF SILICON SURFACES : THE EFFECTS OF A LOW LEVEL BACKGROUND LIGHT

by

**Taposh Kumar Gayen**

The performance of high speed optoelectronic and microelectronic devices largely depends on the uniqueness and development of the fabrication technology. Laser ablation has proven to be an effective three dimensional surface patterning technology. In this thesis, we present findings on the patterning of semiconductor surfaces using laser ablation in air as well as in solutions.

In this thesis, we suggest that the depth of a pattern induced on silicon by firing a pulsed excimer laser in air varies almost linearly with the number of pulses. We report that a He-Ne laser as a background light source has virtually little or no effect on the etching rate. We also suggest that a background light enhances the etching process induced by the excimer laser in wet chemical etching when using a thin-film cell configuration. Pattern depth profiles have been measured by scanning electron microscopy (SEM). We verify our SEM findings by using a light diffraction measurement technique. Finally, we report on the effect of patterning on the electrical properties of metal-semiconductor contacts. Schottky barriers measured for grooved surface showed, in general, a decrease in the barrier height.

# LASER ABLATION OF SILICON SURFACES : THE EFFECTS OF A LOW LEVEL BACKGROUND LIGHT

by
Taposh Kumar Gayen

A Thesis
Submitted to the Faculty of
New Jersey Institute of Technology
in Partial Fulfillment of the Requirements for the Degree of
Master of Science in Engineering Science

Committee for the Interdisciplinary Program in
Materials Science and Engineering

October 1993

## APPROVAL PAGE

# LASER ABLATION OF SILICON SURFACES : THE EFFECTS OF A LOW LEVEL BACKGROUND LIGHT

**Taposh Kumar Gayen**

---

Dr. Haim Grebel, Thesis Advisor — date
Associate Professor of Electrical Engineering, NJIT

---

Dr. Roland A. Levy, Committee Member — date
Director of Materials Science and Engineering Program,
and Professor of Physics, NJIT

---

Dr. David S. Kristol, Committee Member — date
Director of Engineering Science Program,
and Professor of Chemistry, NJIT

## BIOGRAPHICAL SKETCH

**Author :** Taposh Kumar Gayen

**Degree :** Master of Science in Engineering Science

**Date :** October 1993

**Secondary Education :** Dhaka College, Dhaka, Bangladesh

**Undergraduate and Graduate Education :**

- Master of Science in Engineering Science,
  New Jersey Institute of Technology, Newark, NJ, 1993

- Bachelor of Science in Metallurgical Engineering,
  Bangladesh University of Engineering and Technology, Dhaka, Bangladesh
  1989

**Major :** Engineering Science

This thesis is dedicated to
the children of Bangladesh

# ACKNOWLEDGMENT

The author wishes to express his sincere gratitude to his thesis supervisor, Professor Haim Grebel, for his invaluable guidance, assistance, and moral support during the course of this thesis.

Special thanks to Professors Roland A. Levy and David S. Kristol for their final correction and serving as members of the committee.

The author highly appreciates Mr. Joseph of Stevens Institute of Technology for technical assistance and cooperation.

## TABLE OF CONTENTS


| Chapter | Page |
|---|---|
| 1 INTRODUCTION | 1 |
| 2 THEORY | 11 |
| 2.1 Laser Ablation in Air | 11 |
| 2.1.1 Basic Concepts of Laser Ablation | 11 |
| 2.1.2 Absorption of Laser Light | 11 |
| 2.1.3 Laser Induced Heating | 12 |
| 2.1.4 Laser Induced Melting and Evaporation | 14 |
| 2.2 Laser Induced Electrochemical Etching | 15 |
| 2.2.1 Basic Concepts of Light-induced Etching | 15 |
| 2.2.2 Development of the Semiconductor/Electrolyte Interface | 15 |
| 2.2.3 Chemistry of Etching in Solutions | 16 |
| 2.2.4 Effect of Illumination on Charge Transfer | 16 |
| 2.3 Periodic Patterning | 19 |
| 2.3.1 Concept of Periodic Patterning and Diffraction Grating | 19 |
| 2.4 Meatl/ Semiconductor Contact | 22 |
| 3 EXPERIMENTS | 25 |
| 3.1 System Set-up for Laser-aided Interaction with Silicon Surface | 25 |
| 3.1.1 System Set-up | 25 |
| 3.1.2 The Laser System | 27 |
| 3.2 Material Preparation | 27 |
| 3.2.1 Surface Treatment | 27 |
| 3.2.2 Electrolytes | 28 |
| 3.3 Laser Ablation | 29 |
| 3.3.1 Laser Ablation in Air | 29 |

Chapter page

3.3.2 Thin-Film Cell Configuration........................................................ 29

3.4 Measurement of Groove Profile.......................................................... 31

3.4.1 Techniques for the Measurements............................................... 31

3.4.2 Diffraction Modes Measurement................................................. 31

3.5 Meatl-Semiconductor Contact Preparation........................................... 32

3.5.1 Schottky-Barrier and Ohmic Contact........................................... 32

3.5.2 Barrier Height Measurement of Metal/Semiconductor Contact..... 32

4 EXPERIMENTAL RESULTS ............................................................... 34

4.1 The Grating Groove Profile Measurement ........................................... 34

4.1.1 The Grating Profile Due to Ablation in Air.................................. 34

4.1.2 The Grating Profile Due to Wet Chemical Etching....................... 35

4.2 Grating Depth Evaluation by Diffraction Measurement Technique......... 37

4.2.1 The Analysis of Grating profile .................................................. 37

4.3 Barrier Height Measurement............................................................... 38

5 DISCUSSION........................................................................................ 93

6 CONCLUSION....................................................................................... 96

REFERENCES......................................................................................... 97

## LIST OF TABLES


Table | Page

4.1 Light Diffraction Intensity Measurement data from grooves of Samples 1 and 2.( The incident angle $\phi_i$ of the probe beam HeNe ($\lambda$= 633 nm) is 17.31° and the measurement distance [d] is 265 mm ).................. 81

4.2 Light Diffraction Intensity Measurement data from grooves of Samples 3 and 4.( The incident angle $\phi_i$ of the probe beam HeNe ($\lambda$= 633 nm) is 17.31° and the measurement distance [d] is 265 mm).................. 82

4.3 Light Diffraction Intensity Measurement data from grooves of Samples 5 and 6.( The incident angle $\phi_i$ of the probe beam HeNe ($\lambda$= 633 nm) is 17.31° and the measurement distance [d] is 265 mm).................. 83

4.4 Light Diffraction Intensity Measurement data from grooves of Samples 7 and 8.( The incident angle $\phi_i$ of the probe beam HeNe ($\lambda$= 633 nm) is 17.31° and the measurement distance [d] is 265 mm).................. 84

4.5 Light Diffraction Intensity Measurement data from grooves of Samples 9 and 10.( The incident angle $\phi_i$ of the probe beam HeNe ($\lambda$= 633 nm) is 17.31° and the measurement distance [d] is 265 mm).................. 85

4.6 Metal-Semiconductor Barrier Height Determination............................... 92

## LIST OF FIGURES


| Figure | | Page |
|---|---|---|
| 2.1 | Reflectance and absorption coefficients as a function of wave length for the crystalline silicon ( ref. [24] )................................................ | 13 |
| 2.2 | Direct and indirect electron transition in semiconductors; (a) direct transition with accompanying photon emission; (b) indirect transition via a defect level.( ref [25] )............................................................. | 13 |
| 2.3 | Energy band diagram due to contact between (a) an electrolyte a semiconductor showing non-equilibrium, (b) a n-type Si (100) and an electrolyte showing equilibrium, (c) a p-type Si(100) and an electrolyte showing equilibrium...................................................... | 18 |
| 2.4 | Formation of a Schottky barrier between (a) a n-type semiconductor with a metal having a larger work-function (b) a p-type semiconductor and a metal having a smaller work function........................................ | 23 |
| 3.1 | Schematic showing the set-up for laser induced patterning .................... | 26 |
| 3.2 | Schematic showing the arrangement for the diffraction mode measurement........................................................................ | 30 |
| 3.3 | Schematic showing the PEC thin-film cell configuration........................ | 30 |
| 4.1 | Scanning electron micro graph showing the groove profole of a n-type Si(100) surface ablated with the KrF laser ( λ=248nm) in air. [10 pulses of the etching beam were used to induce the pattern]......... | 40 |
| 4.2 | Scanning electron micro graph showing the grrove of a n-type Si(100) surface ablated with the KrF laser ( λ=248nm) in air. [20 pulses of the etching beam were used to induce the pattern].......... | 41 |
| 4.3 | Scanning electron micrograph showing the groove profile of a n-type Si(100) surface ablated with the KrF laser ( λ=248nm) in air. [30 pulses of the etching beam were used to induce the pattern].......... | 42 |
| 4.4 | The grating groove depth versus the number of pulses of the incident excimer laser ( λ=248nm) on a n-type Si(100) in air. [ The points were evaluated by SEM measurement].............................................. | 43 |

Figure | Page

4.5 Scanning electron micrograph showing the groove profile of a p-type Si(100) surface ablated with the KrF laser ( λ=248nm) in air. [10 pulses of the etching beam were used to induce the pattern].......... 44

4.6 Scanning electron micrograph showing the groove profile of a p-type Si(100) surface ablated with the KrF laser ( λ=248nm) in air. [20 pulses of the etching beam were used to induce the pattern].......... 45

4.7 Scanning electron micrograph showing the groove profile of a p-type Si(100) surface ablated with the KrF laser ( λ=248nm) in air. [30 pulses of the etching beam were used to induce the pattern].......... 46

4.8 The grating groove depth versus the number of pulses of the incident excimer laser ( λ=248nm) on a p-type Si(100) in air. [ The points were evaluated by SEM measurement].............................................. 47

4.9 Scanning electron micrograph showing the groove depth profile of a p-type Si(100) surface ablated with KrF laser ( λ= 248nm) in air in presence of a background light source, He-Ne laser( λ= 633 nm). [10 pulses were used to induce the pattern]........................................ 48

4.10 Scanning electron micrograph showing the groove depth profile of a p-type Si(100) surface ablated with KrF laser ( λ= 248nm) in air in presence of a background light source, He-Ne laser( λ= 633 nm). [ 20 pulses were used to induce the pattern]................ 49

4.11 Scanning electron micrograph showing the groove depth profile of a p-type Si(100) surface ablated with KrF laser ( λ= 248nm) in air in presence of a background light source, He-Ne laser( λ= 633 nm). [30 pulses were used to induce the pattern].................................. 50

4.12 The grating groove depth versus the number of pulses of the incident excimer laser ( λ=248nm) on a p-type Si(100) in air in presence of a background light source [ The points were evaluated by SEM measurement].......................................................................... 51

4.13 Scanning electron micrograph showing the groove profile of a n-type Si(100) surface ablated with the KrF laser ( λ=248nm) in air. [50 pulses of the etching beam were used to induce the pattern].......... 52

| Figure | | Page |
|---|---|---|


4.14 Scanning electron micrograph showing the groove profile of a n-type Si(100) surface ablated with the KrF laser ( λ=248nm) in air.[100 pulses of the etching beam were used to induce the pattern]............... 53

4.15 Scanning electron micrograph showing the groove profile of a n-type Si(100) surface ablated with the KrF laser ( λ=248nm) in air. [150 pulses of the etching beam were used to induce the pattern]...... 54

4.16 Scanning electron micrograph showing the groove profile of a n-type Si(100) surface ablated with the KrF laser ( λ=248nm) in air. [200 pulses of the etching beam were used to induce the pattern]...... 55

4.17 Scanning electron micrograph showing the groove profile of a n-type Si(100) surface ablated with the KrF laser ( λ=248nm) in air. [250 pulses of the etching beam were used to induce the pattern].. 56

4.18 The grating groove depth versus the number of pulses of the incident excimer laser ( λ=248nm) on a n-type Si(100) in air. [ The points were evaluated by SEM measurement]............................................ 57

4.19 Scanning electron micrograph of the etched pattern induced on a p-type Si(100) surface in a thin-film cell configuration in a $KOH:H_2 0::1:20$ solution.[30 pulses of the excimer laser were used to induce the pattern]....................................................................................... 58

4.20 Scanning electron micrograph of the etched pattern induced on a p-type Si(100) surface in a thin-film cell configuration in a $KOH:H_2 0::1:20$ solution in presence of a background illumination of 1.25 mW. [30 pulses of the excimer laser were used to induce the pattern].......... 59

4.21 Scanning electron micrograph of the etched pattern induced on a p-type Si(100) surface in a thin-film cell configuration in a $KOH:H_2 0::1:20$ solution in presence of a background illumination of 2.50 mW. [30 pulses of the excimer laser were used to induce the pattern]......... 60

4.22 Scanning electron micrograph of the etched pattern induced on a p-type Si(100) surface in a thin-film cell configuration in a $KOH:H_2 0::1:20$ solution in presence of a background illumination of 3.75 mW. [30 pulses of the excimer laser were used to induce the pattern].......... 61

Figure | Page

4.23 Scanning electron micrograph of the etched pattern induced on a p-type Si(100) surface in a thin-film cell configuration in a $KOH:H_2O::1:20$ solution in presence of a background illumination of 5.00 mW. [30 pulses of the excimer laser were used to induce the pattern]......... 62

4.24 The grating depth versus total background illumination for the p-type Si(100)/$KOH:H_2O$ system. [ The points were evaluated by SEM measurement; 30 pulses of the excimer laser were used to etch the pattern]........................................................................................ 63

4.25 Scanning electron micrograph of the etched pattern induced on a p-type Si(100) surface in a thin-film cell configuration in a $KOH:H_2O::1:20$ solution.[30 pulses of the excimer laser were used to induce the pattern]........................................................................................ 64

4.26 Scanning electron micrograph of the etched pattern induced on a n-type Si(100) surface in a thin-film cell configuration in a $KOH:H_2O::1:20$ solution in presence of a background illumination of 1.25 mW. [30 pulses of the excimer laser were used to induce the pattern]......... 65

4.27 Scanning electron micrograph of the etched pattern induced on a n-type Si(100) surface in a thin-film cell configuration in a $KOH:H_2O::1:20$ solution in presence of a background illumination of 2.50 mW. [30 pulses of the excimer laser were used to induce the pattern]........... 66

4.28 Scanning electron micrograph of the etched pattern induced on a n-type Si(100) surface in a thin-film cell configuration in a $KOH:H_2O::1:20$ solution in presence of a background illumination of 3.75 mW. [30 pulses of the excimer laser were used to induce the pattern]......... 67

4.29 Scanning electron micrograph of the etched pattern induced on a n-type Si(100) surface in a thin-film cell configuration in a $KOH:H_2O::1:20$ solution in presence of a background illumination of 5.00 mW. [30 pulses of the excimer laser were used to induce the pattern]......... 68

4.30 The grating depth versus total background illumination for the n-type Si(100) / $KOH:H_2O$ system. [ The points were evaluated by SEM measurement; 30 pulses of the excimer laser were used to etch the pattern]................................................................................. 69

Figure | Page

4.31 Scanning electron micrograph of the etched pattern induced on a p-type Si(100) surface in a thin-film cell configuration in a $HF:HNO_3:H_2O$:: 2:3:100 solution. [ 30 pulses of the excimer laser were used to induce the pattern] ........ 70

4.32 Scanning electron micrograph of the etched pattern induced on a p-type Si(100) surface in a thin-film cell configuration in a $HF:HNO_3:H_2O$:: 2:3:100 solution with a background light of 1.25 mW [ 30 pulses of the excimer laser were used to induce the pattern] ........ 71

4.33 Scanning electron micrograph of the etched pattern induced on a p-type Si(100) surface in a thin-film cell configuration in a $HF:HNO_3:H_2O$:: 2:3:100 solution with a background light of 2.50 mW [ 30 pulses of the excimer laser were used to induce the pattern] ........ 72

4.34 Scanning electron micrograph of the etched pattern induced on a p-type Si(100) surface in a thin-film cell configuration in a $HF:HNO_3:H_2O$:: 2:3:100 solution with a background light of 3.75 mW [ 30 pulses of the excimer laser were used to induce the pattern] ........ 73

4.35 Scanning electron micrograph of the etched pattern induced on a p-type Si(100) surface in a thin-film cell configuration in a $HF:HNO_3:H_2O$:: 2:3:100 solution with a background light of 5.00 mW [ 30 pulses of the excimer laser were used to induce the pattern] ........ 74

4.36 The grating depth versus total background illumination forthe p-type Si(100)/ $HF:HNO_3:H_2O$ system. [ The points were evaluated by SEM measurement; 30 pulses of the excimer laser were used to etch the pattern] ........ 75

4.37 Scanning electron micrograph of the etched pattern induced on a n-type Si(100) surface in a thin-film cell configuration in a $KOH:H_2O$::1:20 solution without any background illumination [ 20 pulses of the excimer laser were used to induce the pattern] ........ 76

4.38 Scanning electron micrograph of the etched pattern induced on a n-type Si(100) surface in a thin-film cell configuration in a $KOH:H_2O$::1:20 solution with a background light of 1.25mW [ 20 pulses of the excimer laser were used to induce the pattern] ........ 77

Figure Page


4.39 Scanning electron micrograph of the etched pattern induced on a n-type Si(100) surface in a thin-film cell configuration in a $KOH:H_2 0::1:20$ solution with a background light of 3.75mW [ 20 pulses of the excimer laser were used to induce the pattern]............................... 78

4.40 Scanning electron micrograph of the etched pattern induced on a n-type Si(100) surface in a thin-film cell configuration in a $KOH:H_2 0::1:20$ solution with a background light of 5.00 mW [ 20 pulses of the excimer laser were used to induce the pattern]............................... 79

4.41 The grating depth versus total background illumination for the n-type Si(100)/$KOH:H_2 0$system. [ The points were evaluated by SEM measurement; 20 pulses of the excimer laser were used to etch the pattern]........................................................................................ 80

4.42 The grating depth vs total background illumination for the n-type Si(100) / $KOH:H_2 0$system. [ The points were evaluated by SEM measurement; only 1 pulse of the excimer laser was used to etch the pattern]........................................................................................ 86

4.43 Forward current-voltage (I-V) characteristics of Al/p-type Si(100) contacts both on the patterned and flat surfaces of the sample number1........................................................................ 87

4.44 Forward current-voltage (I-V) characteristics of Al/p-type Si(100) contacts both on the patterned and flat surfaces of the sample number 2........................................................................ 88

4.45 Forward current-voltage (I-V) characteristics of Al/p-type Si(100) contacts both on the patterned and flat surfaces of the sample number 3 ........................................................................ 89

4.46 Forward current-voltage (I-V) characteristics of Al/p-type Si(100) contacts both on the patterned and flat surfaces of the sample number 4 ........................................................................ 90

4.47 Forward current-voltage (I-V) characteristics of Al/p-type Si(100) contacts both on the patterned and flat surfaces of the sample number 5 ........................................................................ 91

# CHAPTER 1

# INTRODUCTION

Laser ablation and laser chemical processing of materials have received much attention in recent years. In any laser processing, unique properties-high spatial and temporal coherence- of a laser manifest themselves as a set of related parameters (spatial profile, temporal profile, power density, wave length, coherence length, optical bandwidth ) that determine the nature of interaction of the laser with the rest of the system [1]. The excimer laser, due to its high power and multiple available wavelengths in the ultraviolet region, has made itself an excellent tool for the fabrication and processing of materials.

Laser ablation has been successfully used to deposit a wide range of materials including dielectrics, semiconductors, metals, and superconductors [2]. Pulsed-laser ablation under vacuum gives film stoichometry close to the target maintaining its unique advantage of relative simplicity, minimum of hardware, and safety by comparison to photo-CVD [3] which requires various toxic gas sources. In addition to this, modification in the composition of the deposit and formation of new compounds have been achieved by working in a reactive atmosphere [4].

Laser ablation, both in air and in vacuum, refers to rapid thermal melting and / or evaporation of materials by firing a high power UV laser with little chemistry involved. The main objective of this approach is that materials to be removed from the appropriate region of the target sample as efficiently as possible. In fact, the most desirable aspect of this operation is the ability to localize annealing or surface treatment. The aim of this process is to introduce the appropriate amount of energy into the sample in order to melt and evaporate right amount of materials to achieve the required pattern or structure, or the both.

The high mass ablation rate of the material depends on the favorable performance in two areas of laser-plasma interaction physics: first, obtaining the highest absorption rate, and second, minimizing the generation of supra thermal electrons. This, in turn, has been found to be sensitive to the characteristics of the incident laser pulse. Absorption, on the other hand, as a measure of mass ablation efficiency, is found to be related with the laser intensity, the pulse duration , and the wavelength [5].

A large body of experimental work on pulsed laser ablation and annealing of silicon surfaces has been done to find different threshold energy fluences for heating the substrate, for annealing and damaging the sample, and for plasma formation and getting the absorption spectra for silicon particle clouds. Different time-resolved (TR. ) techniques have been used to indicate the effects of intense picosecond or nanosecond pulsed-laser irradiation of silicon. In order to clarify the nature of fast phase transitions already mentioned, such as pulsed-laser annealing and explosive crystallization , it is important to study both electronic and geometric structures of l-Si [6]. The appearance of spontaneous periodic surface structures, or ripples have been studied to know the final effect of the pulsed-laser ablation.

Pulsed-laser annealing of silicon has been done at various wavelength, mostly in the range between 248 and 1064 nm [7]. Some experimental findings are presented here to quantify the energy and time dependence of annealing process and to determine the energy density range within which annealing takes place. In the range I, from 0 up to 0.17 J/cm$^2$, the sample is just heated, not annealed. In the range II, from 0.17 to 1 J/cm$^2$, annealing takes place. Range III, above 1 J/cm$^2$, is the damaging range. In range III, sharp line structures appear in the absorption spectra above the L $_{II,III}$ edge, between 110 and 150 eV, and the L $_{II,III}$ edge shifts

to higher energies, compared to the edge position for the un-irradiated foil ( 110 eV, instead of 100 eV) [8].

The emission of the particles - as Si atoms, or as small sized clusters and/or as Si ions - from the surface depends on the energy density of the laser used. However, the size of the clusters is approximately 5 to 10 atoms per cluster. Depending on the particle production two distinguishable energy density regions are found. Actually these two regions are the subdivision of the range III . In the low-energy density region, liquid clusters (droplets ) are emitted from the surface due to the thermal strain of the superheated subsurface layer and in the high -energy density region the plasma is formed, which emits electrons and subsequently ions by the repulsive Coulomb force. The neutral atoms are emitted from the interface of these two regions [9]. According to the work of H. Van Burg et al. [8] following results were achieved : at 3.5 $J/cm^2$ most emitted particles were large sized clusters (droplets ) and neutral Si atoms. At 6.0 $J/cm^2$ there were small clusters, Si atoms, and $Si^{1+}$ ions. At 14 $J/cm^2$ ionized silicon upto $Si^{4+}$ were detected. And with even higher energy-density $Si^{5+}$ were found.

The appearance of surface ripples and changes in the morphology due to the irradiation of picosecond or nanosecond pulse lasers has already been reported [7]. Morphology change or surface damage has been found to occur at the irradiated area as a result of melting and subsequent crystallization [10]. Young et al. [11] have reported that surface ripples perpendicular to the polarization of the radiation with spacing of approximately the laser wave length can be achieved at laser fluences just above the melting threshold. This generation of the ripple pattern has been attributed to interference between scattered surface waves and the incident polarized laser radiation. At higher fluences, other effects associated with non

uniform melting, rapid solidification, sputtering, and evaporation appear to govern the damage process.

Calorimetric, acoustic, and morphological studies done by Gorodetsky et al [7] of silicon have reported the following findings : (a) The calorimetric measurements suggest that there is no effect of the optical reflectivity change on entering the molten phase, nor any loss of energy due to subsequent fast re solidification to an amorphous phase, (b) there is a large enhancement of the acoustic signal at the damage threshold due to large volume change on melting, (c) the surface damage morphology indicates the evidence of both standing acoustic and capillary waves.

In the first part of the thesis, we have indicated the depth profile of silicon, both p-type and n-type, surfaces ablated by an excimer laser ( $\lambda$ = 248 nm ) as a function of number of pulses, and have found that the depth of the profile varies almost linearly with the number of pulses pulses. We have also demonstrated that the background illumination He-Ne ( $\lambda$= 633 nm ) has virtually no effect on the ablation efficiency of the excimer laser. Melting, evaporation, and rapid solidification of the melt have also been reported.

Laser-induced chemical processing has suggested its use for basic improvements in the conventional fabrication technology and, even more important, for the fabrication of new forms of micro structures, devices, and integrated circuits (IC's). Laser-chemical processing has demonstrated its superior ability of performing the four basic ingredients of IC fabrication - growth, deposition, etching, and doping. Unusual results obtained with laser processing has suggested it as a novel device. Three areas will be presented here to demonstrate the practical laser-based application.

First, laser chemical processing has successfully been used to repair reticles for photolithographic patterning [12]. In photolithiographic masks two types of defects, transparency (absence of metallization) and opacity (presence of excess metallization) have been identified. Laser deposition and laser ablation can correct the defects- transparency and opacity respectively. Second, laser-induced chemical processing has been used to fabricate components for opto-electronic devices from compound semiconductors [13]. Currently most of the laser-enhanced chemical processings have been directed towards the fabrication of Bragg distributed - feedback (DFB) elements for diode lasers. Third, focused laser chemistry has rendered more flexibility in direct writing than existing methods, such as electron beam writing in photoresist, electron- or laser-beam latching of transistors.

Laser-induced chemical processings can be categorized as : low-temperature processing, maskless patterning, and beam-controlled anisotropy on the basis of their unique capabilities. Low temperature processing is extremely important where slight dimensional changes due to temperature rise can deteriorate the device performance. Laser processing can minimize heating by confining laser beam to a small spatial region, and dissociating a molecule efficiently by direct absorption, via a process known as multiphoton absorption [ 14, 15]. Laser chemical processing can generate pattern on the substrate surface without any need of masking, and can do so only in one step. In any standard planer processing, patterning of a doped region on a semiconductor wafer is a complex process involving as many as ten or more steps. Maskless writing of doped, etched, and deposited lines is an entirely new processing capabilities [1]. Laser beam processing can be anisotropic; independent of crystal orientation. Laser processing anisotropy arises from two phenomena : (a) non linearity in process rate with high local light intensity, (b) wave guiding of the laser beam by the patterned , etched surface.

Laser chemical processing is effected by two processes determined by wavelength and bandwidth. The first approach, known as photolytic process, is a direct, nonthermal interaction of the laser photons with the electronic structure of the material through single or multiphoton excitation. The second approach, known as pyrolytic process, refers to a state of non equilibrium . In this approach the laser acts as a directed heat source, either on the solid materials directly, or indirectly via a local surface, to produce a near thermal distribution of the excited species. In laser chemical processing, the end product in either case is to dissociate the molecular precursors to form the final products , such as a dopant or etchant species. The whole excitation process and the dissociation process are controlled spatially to confine material and thermal diffusion.

Laser-induced etching, on the basis of electron-hole pair generation, of semiconductor can be effected by three methods. The first method is photochemical etching under anodic polarization. The etching rate, with n-type semiconductor electrodes in the limiting current regime, is controlled by the availability of holes. Illumination serves as additional source of holes, so illuminated areas dissolve faster than non illuminated areas. The second one is the illumination of a semiconductor in a non oxidizing solution without any external biasing. Non uniform illumination produces difference in the surface potential and minority carrier concentration. The illuminated regions, in n-type semiconductors, act as local anodes and are dissolved, whereas the nonilluminated areas act as local cathode; therefore reduces oxygen and produces hydrogen. The third method is the illumination of a semiconductor in an oxidizing solution without any external biasing. The etch rate is limited by the supply of minority carriers. However, the etching occurs in both the illuminated and nonilluminated areas . But an accelerated etching rate is observed in the illuminated areas.

Etching reactions occur in several steps and the dissolution rate depends upon the nature of rate limiting step of the etching process. The rate-limiting step can be activation controlled or can be mass transport controlled. When the rate of the reaction is determined by the chemical activity of the species involved, then the process is said to be reaction limited or activation controlled. On the other hand, if the rate is controlled by the speed at which etchant and reception products are transported from one place to the other, then the reaction is said to be diffusion-limited or mass-limited etching.

The etching reaction is favorable in one direction of the crystal than the other. The anisotropy arises due to the difference in the surface activity of the different crystal planes. As for example, the etching rate of GaAs in $H_2SO_4 : H_2O_2 : H_2O$ : : 8: 1: 1 solution is 0.8 micron/min for the (111) A face and 1.5 micron/ min for all other faces [16]. Wet-chemical laser etching can produce vertical, high-aspect features that are required in the fabrication of advanced electronic, electrooptical, and micromechanical devices. The vertical etching can avoid the undercutting of the adjacent structures as demanded by modern integrated circuits of close spacing. The third dimension of a semiconductor is currently being investigated as a means of providing additional interconnections from the front to the back of the wafer. This very intention stems from three basic goals : to reduce the length of connections between devices for faster processing rate; to reduce the interference and crosstalk between interconnections; and to reduce the area occupied by interconnections on the surface of the semiconductor wafer [17].

Etching rate and / or time has been found to be dependent on the laser intensity, concentration of the etching solution, temperature, grating spacing, and the external biasing of the thin-film cell. H. Grebel et al. [18] have shown that in a liquid-phase thin-film cell configuration a minimum etching time can be achieved

with an optimum electrolyte concentration and a given laser intensity. In the article, it has also been reported that as the laser intensity increases , an apparent saturation of the etching time is achieved. Application of an external potential biasing can reduce the etching time substantially if the etchant concentration is relatively low. Turner et al. [19] have reported that laser-induced etching rate can increase by a factor of two for a modest 10°C increase in the temperature. In fact, the laser acts as a localized heat source which thermally activates the reaction. Finally, for smaller-spacing gratings, i.e., $\leq$ 1- μm etching rate decreases due to the lateral carrier diffusion on the surface.

Grating depth profile has been found to be dependent upon the grating spacing. Podlesnik et al. [20 ] have reported that the higher the grating spacing the higher the groove depth for a particular etching time. The aspect ratio increases as the grating spacing increases. For submicron grating spacings, the aspect (depth-to-spacing) ratio was found to be 0.2 and with grating spacings $>$ 1-μm, the aspect ratio was found to exceed 0.4; and the ratio was 0.8 for grating of 2-μm.

Podlesnik et al. [20] and S. Ida et al. [21] have found out the reasons and explanations for different types of groove profiles. They believe that after the grooves attain a specific surface morphology, the photogenerted holes diffuse spatially such that a constant etching rate at each point of the the groove profile is maintained. Although the unmodulated etching continues at a constant rate, yet the groove profile does not change. The profile of the grating grooves depends on the details of the carrier movement within the semiconductor, the relative magnitude of the dark versus light-enhanced etching rate, and the anisotropy in the etching process. Generally, gratings with spacings $>$ 1 μm had a sinusoidal profile due a linear dependency between etching rate and light distribution on the surface. On the other hand, submicrometer grating shows a deviation from simple sinusoidal profile

and exhibits a cusped profile. This sort of groove profile has generated due to local variations in the hole drift caused by photoinduced electric fields, both normal and transverse to the surface. The second type of groove profile, the blazed grating can be accomplished by tilting the substrate. The deviation from right angle represents the blazed angle. The tilting of the substrate in conjunction with the continuous dark etching produces a clear, blazed profile. The profile can be triangular or cusped depending on the relative magnitude of the uniform and light-enhanced etching rate. The third type, the impulse profile can be achieved using a solution of 10 times higher $H_2O_2$ content than the normal solution $H_2O_2$: $H_2SO_4$: $H_2O$ = 1:1:100 and a laser power density of 1 kW/cm$^2$ . Extremely fast etching rate under this condition produces this type of anisotropic profile.

In the second part of this thesis, we have studied the excimer ( $\lambda = 248$ nm) laser-induced wet chemical etching of p-type and n-type of Si (100) both in KOH-$H_2O$ and in HF : $HNO_3$ : $H_2O$ solution systems. We have reported the depth of the etched profiles with the variation of number of pulses. We have also reported the effect of background illumination of He-Ne ( $\lambda = 633$ nm ) laser on the etching efficiency of the excimer laser. We have established that secondary illumination has an enhanced effect on the etching reaction contradictory to the findings of Willner et al. [22].

Metal/semiconductor interface is an important subject in microelectronic technology because every semiconductor device needs the interface to communicate with other circuits. There is an urgent need to improve the quality of ohomic contacts as well as Schottky contacts for better performance of high-speed as well as optoelectronic devices [23]. In devices where the electrical characteristics of the Schottky diodes govern the device performance, it is important to find a metal with a high barrier height, excellent ideality factor, metallurgical stability and a fabrication

process which is reproducible. In the third part of this thesis, we have demonstrated that by simply patterning the surface of the semiconductor before making the metal/semiconductor contacts the barrier height can be decreased increased. This achievement might obviate the stringent need to get a unique metal for metal/semiconductor contacts.

Generally, most of the useful properties of a p-n junction can be exploited by simply making a suitable metal/semiconductor contact. This metal/semiconductor contact can be rectifying ( Schottky barrier ) or may be nonrectifying ( ohmic contact). A Schottky-barrier is formed when an n-type semiconductor makes a contact with a metal having a larger work function or a p-type semiconductor makes a contact with a metal having a smaller work function [24]. A Schottky barrier is rectifying because it allows easy flow of current in the forward direction and little current in the reverse direction. The current transport in this type of contact is mainly due to the injection of majority carriers from semiconductor into the metal. On the other hand, an ohmic contact is non-rectifying because it has no tendency to rectify signals and allows easy flow of current in the either direction.

In the last part of the thesis, we have demonstrated the effect of patterning on the electrical properties of the metal/semiconductor contacts. We have made pattern on the front surface of p-type Si (100) and then we have put Al-contact on it in the form of a thin film by the technique of the metal-vapor deposition. On the back side of Si the contact with Al was followed by laser annealing. The effect of periodicity and depth of the patterning on the metal/semiconductor contact have been presented here. The difference in the barrier heights due to patterning have been explained carefully.

# CHAPTER 2

# THEORY

## 2.1 Laser Ablation in Air

### 2.1.1 Basic Concepts of Laser Ablation

The basis of interaction of the materials with a laser beam is that the electromagnetic energy of the laser is converted first into electronic excitation and then into thermal, chemical and mechanical energy. The interaction ultimately changes the electronic structure as well as the shape of the materials in different ways [25].

### 2.1.2 Absorption of Laser Light

The efficient performance of laser ablation / fusion applications requires favorable performance in two areas: first, obtaining the highest absorption rate, and second , minimizing the generation of suprathermal electrons. However, it turns out that absorption is the most critical step in laser processing. The absorption increases when the laser intensity increases, absorption increases when the pulse duration increases, and absorption increases when the wavelength decreases [5]. These facts again can be interpreted by reflection and absorption coefficients that virtually determine the amount of beam power absorbed within the material. **Figure 2.1** shows the absorption coefficient and the reflectance as a function of wavelength for crystalline Si (Eg = 1.1 eV at room temperature, corresponding to $\lambda$ = 1.13 micron) [24]. Crystalline silicon exhibits the essential features-the absorption peaks appear around 10 $\mu$m due to phonon coupling, weak absorption at intermediate wavelengths and a steep increase in absorption as the photon energy approaches the band gap.

Corresponding to **Figure 2.1**, it can be noted that the absorption coefficient of Si increases with decreasing laser wave-length only gradually near 1.13μm ( hω = 1.1 eV), but rather abruptly near 0.36 μm ( hω = 3.4 eV ). This difference exhibited in Si can be interpreted by two different types of interband transitions. **Figure 2.2** shows these transitions [25]. In the first kind, the transition between the valence-band and conduction-band occurs at the same wave-vector, known as direct transition. Such transition is possible in Si only at photon energies exceeding its direct gap at 3.4 eV. The second kind of transition, the indirect transition, involves valence - and conduction- band states of different wave vector. The difference in the wave vector is provided by a phonon, as photon itself carries little momentum. The probability of such transitions depends on the phonon occupancy and is relatively small and temperature dependent [25].

### 2.1.3 Laser Induced Heating

The primary effect of absorbed laser light is not heat but particle excess energy-excitation energy of bound electrons, kinetic energy of free electrons, and excess phonon. Once energy has been coupled into the carrier system, it must be redistributed among the other carriers. The distribution of the ordered and localized primary excitation energy into uniform heat takes place into three steps. The first step is spatial and temporal randomization of the motion of the excited particles, proceeding with collision time of the particles. This time is even shorter than the duration of the shortest pulsed lasers. The second step, energy equipartition, tends to involve a large number of elementary collisions. Several energy transfer mechanisms can be traced, each involving its own characteristic time constant. For example, for hot carriers in nonmetals, the time constant for energy distribution by phonon emission in the conduction band is different from that of the time constant

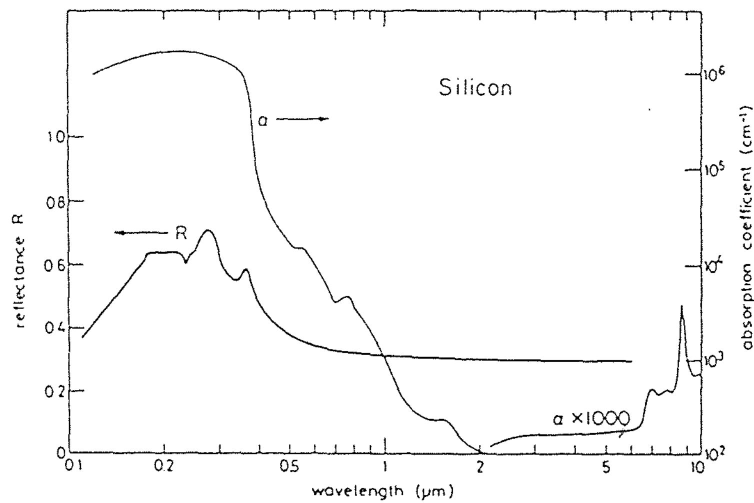


**Figure 2.1** Reflectance and absorption coefficients as a function of wavelength for the crystalline silicon. ( ref. [24] ).

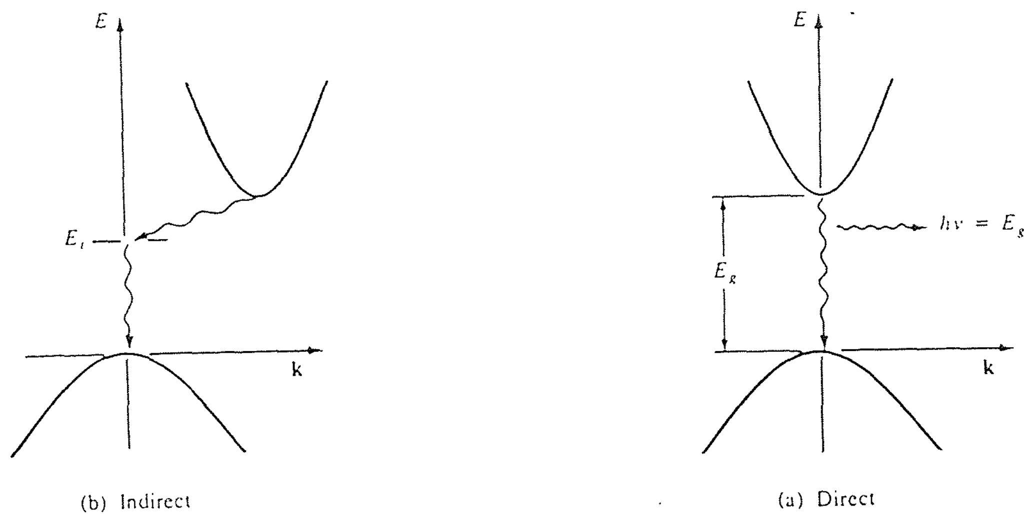


**Figure 2.2** Direct and indirect transitions in semiconductors; (a) direct transition with accompanying photon emission; (b) indirect transition via a defect level. (ref. [25])

by recombination. The third step is the heat flow stage. Once the laser energy is converted to heat it still remains to be highly localized on a macroscopic level. The one-dimensional heat-flow equation can be used to interpret this heat-conduction phenomenon. However, the scattering processes are extremely rapid. The lattice may be heated up by rapid phonon scattering instantaneously as a consequence of direct irradiation by intense laser beams.

### 2.1.4 Laser Induced Melting and Evaporation

It is very difficult to estimate the power required to achieve a desired processing temperature because of the large nonlinearities associated with laser heat of silicon. However, it is not difficult to determine if melting or evaporation occurs by the experiment. Thus, the power of incident laser beam can be determined. Gorodetsky et al. [7] have already reported that melting of silicon is evident at the lowest energy density, which is well above the melting threshold of $\approx$ o.13 $J/cm^2$ for silicon with ArF excimer laser irradiation. However, measurable ablation has not occurred below a threshold energy density of $\approx 1.3\ J/cm^2$ , which corresponds to a power density of $\approx 7.2 \times 10^7\ W/cm^2$ for an 18 ns laser pulse duration and to a power density of $\approx 9.3\times 10^7\ W/cm^2$ for a 14 ns ArF laser pulse.

Poprawe et al. [27] have already characterized three different mechanisms for material removal depending on the incident laser intensity. At power densities sufficient to liquefy the material, but below the vaporization threshold , material is removed at very low rates according to the vapor pressure above the liquid. If the energy density is above the vaporization threshold, a dense vapor develops above the surface. Initially ionization due to multiphoton processes rapidly converts the vapor into plasma. Finally this plasma becomes dense enough so that further absorption is dominated by inverse bremsstrahlung. As the energy density in plasma

increases and pressure waves propagating to the surface become sufficiently large, then rapid expulsion of materials occur from the liquefied zone. These shock waves are called laser supported combustion waves (LSC waves) and are accompanied by pressure of several hundred bar. The result is a rapid increase in material removal rate with increasing laser intensity. At still higher laser intensities, the plasma becomes so dense that absorption occurs almost entirely in a small zone confined to the top of plasma causing explosive heating of the region, thereby initiating laser supported detonation waves (LSD waves). Due to inefficient coupling between laser energy and the surface the ablation rate does not increase linearly with increasing laser intensity.

## 2.2 Laser Induced Electrochemical Etching

### 2.2.1 Basic Concept of Light Induced Etching

Laser-induced etching of semiconductors is electrochemical in nature. It is a process in which the material is converted into a soluble compound [28]. The PEC etching involves three steps: the generation of photoinduced carriers, reaction of the carriers with the ionic species of the electrolyte at the interface of semiconductor/electrolyte leading to the formation of oxides, and the dissolution of the oxides into the electrolyte and their transport away from the surface [29].

### 2.2.2 Development of the Semiconductor/Electrolyte Interface

When a semiconductor is brought in contact with an electrolyte, band bending occurs due to the energy differences in the Fermi level. In equilibrium, without laser irradiation, the Fermi level of the semiconductor must match the Fermi/redox level of the electrolyte and the vacuum levels of the two must be continuous. As a result,

the semiconductor bands will be bent upwards or downwards, depending on whether the semiconductor is n- or p-type. This is shown in **Figure 2.3.**

### 2.2.3 Chemistry of Etching in Solutions

Any etching process, involves oxidation-reduction reactions, and is followed by dissolution of the oxidation products. An example in this regard will clarify the whole process. The semiconductor is converted to a higher oxidation state at a localized anodic site by the reaction :

$$M^{o} + nh^{+} \rightarrow M^{n+} \qquad (2.1)$$

Where $M^{o}$ represents the semiconductor material, and $M^{n+}$ its oxidation product. The oxidation reaction requires n holes for its execution. Reduction reaction occurs simultaneously at a localized cathodic site, and is accompanied by consumption of electrons :

$$N^{o} + ne^{-} \rightarrow N^{n-} \qquad (2.2)$$

where $N^{o}$ represents the oxidation and $N^{n-}$ is its reduced state. The overall reaction, which is charge neutral , is given by :

$$M^{o} + N^{o} \rightarrow M^{n+} + N^{n-} \qquad (2.3)$$

Unless there is any external biasing, it is very hard to locate anode or cathode. But in most of the cases etching done under biasing.

### 2.2.4 Effect of Illumination on Charge Transfer

The illumination of semiconductor surfaces by photons above the bandgap can lead to the chemical reaction when the sample is immersed in a solution. Electron-hole pairs are created in the semiconductor which then separate in the space charge

(depletion) layer of the semiconductor created by the semiconductor-electrolyte interface; the charge carriers are injected into the semiconductor-electrolyte interface to drive oxidation or reduction reaction [ 30]. Williams and Nozik [ 31] have approximated the region of the semiconductor-electrolyte interface as a semiconductor heterojunction and focused attention on the irreversibilities associated with minority charge carrier injection. The irreversibility due to photoinjection into the electrolyte arises from the strong electronic-vibrational interaction in the electrolyte. **Figure 2.3** shows the band diagram in this case.

Due to irradiation of KrF laser on silicon thin-film cell configuration, carrier transport across the interface of the semiconductor/electrolyte occurs. Silicon, in our case, is oxidized into a higher oxidation state by the reaction :

$$Si + 2h^{+} \rightarrow Si^{2+} \qquad (2.4)$$

The oxidation reaction requires two holes for its execution. The primary oxidizing species in semiconductor etching is $OH^-$ which is the dissociation product of water:

$$H_2O = OH^- + H^+ \qquad (2.5)$$

The $Si^{2+}$ in Eq 2.5 combines with $OH^-$ to give

$$Si^{2+} + 2OH^- \rightarrow Si\,(OH)_2 \qquad (2.6)$$

which subsequently liberates hydrogen to form $SiO_2$ :

$$Si(OH)_2 \rightarrow SiO_2 + H_2 \qquad (2.7)$$

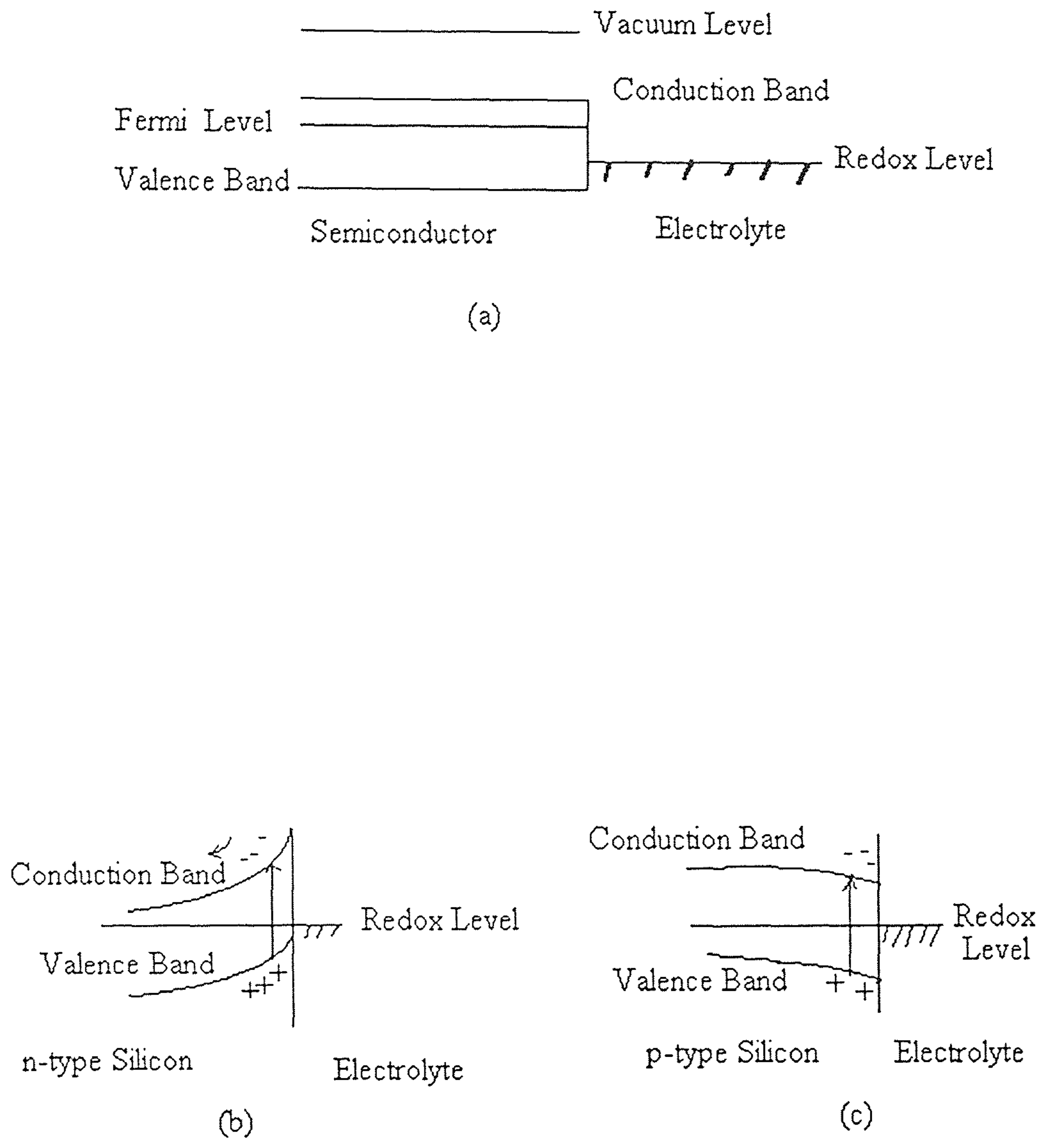


**Figure 2.3** Energy band diagrams between (a) a semiconductor and an electrolyte showing non-equilibrium; (b) a n-type Si(100) and an electrolyte under illumination showing equilibrium; (c) a p-type Si(100) and an electrolyte under illumination showing equilibrium. [ The charge carriers flow under illumination with band-gap radiation is indicated].

Hydrofluoric acid/ potassium hydroxide is used to dissolve $SiO_2$. The reaction is :

$$SiO_2 + 6\,HF \rightarrow H_2SiF_6 + H_2O \qquad (2.8)$$

Where $H_2SiF_6$ is soluble in water.

## 2.3 Periodic Pattering

### 2.3.1 Concept of Periodic Pattering and Diffraction Grating

'Periodic patterning' induced on the semiconductor surface by laser-aided chemical etching can be best elucidated by the basic concept of diffraction grating. Two equal-intensity laser beams with incident angle $2\phi_i$ intersecting on the semiconductor surface can form the grating with period $\Lambda$ [32]

$$\Lambda = \frac{\lambda}{2nSin\,\phi_i} \qquad (2.9)$$

where $\lambda$ is the wavelength of the incident laser beam and n is the refractive index of air. The concept of phase grating might throw more light on the understanding of periodic patterning.

A phase grating can be defined by the reflectance function [33, 34] :

$$r(x) = \exp\,[\,j\,m\,f\,(\,Kx)] \qquad (2.10)$$

where

$$m = ny\,\frac{\pi}{\lambda}\,(\,\cos\phi_i + \cos\phi_r) \qquad (2.11)$$

The parameter m is the modulation coefficient, it represents the peak-to-peak excursion delay, n is the refractive index of the electrolyte, $\phi_i$ and $\phi_r$ the incident and reflected angle of the monitoring beam and $K = 2\pi/\lambda$ . The function mf ( Kx) represent the real profile of the grating and $\lambda$ is the wave vector of the pattern.

The reflectance function of a sinusoidal phase grating can be defined as: $r(x) = \exp [ j\ m \sin (Kx)]$ and the field strength in the Fraunhofer diffraction pattern can be written as the Fourier transform of the reflectance function :

$$U(x_o) = \tau [ r(Kx)] \quad (2.12)$$

$$= \tau [\exp( j\ m \sin ( Kx))] \quad (2.13)$$

$$= c \sum_{\infty}^{\infty} Jq (m) \quad (2.14)$$

where c is a constant which depends on the wavelength of the measuring source and the distance from the recording medium, and Jq is the Bessel function of the $q^{th}$ order . The grating efficiency of the $q^{th}$ order can be represented as :

$$\frac{I_q}{I_{00}} = [Jq (m )]^2 \quad (2.15)$$

where $I_q$ is the intensity of the $q^{th}$ diffracted mode, and $I_{oo}$ is the specular reflection. The position of the qth diffracted order can be presented by :

$$\text{Sin}\ \phi_q - \text{Sin}\ \phi_i = \frac{1}{d}[Xq - Xi] \quad (2.16)$$

where $\phi_q$ is the qth order diffracted angle.

In general a periodic function with $|e^{j\phi}| \equiv 1$ is :

$$r(x) = \exp[\, j\, m\, f(Kx)] \tag{2.17}$$

$$= \sum_{q=-\infty}^{\infty} Cq \exp(jqKx) \tag{2.18}$$

It is assumed that each diffraction mode is fully separated. The coefficients $C_q$ can be found from the intensity of the diffracted order :

$$Cq = \pm\,(I_q / I_{00})^{1/2.} \tag{2.19}$$

The exact profile depth can be found by measuring the intensity of the first order light intensity diffraction from an ideal sinusoidal etched pattern and defining the etching efficiency :

$$\eta = \frac{I_1}{I_{00}}$$

$$= J_1^{\,2}[\frac{1}{2} kny(\cos\phi_i + \cos\phi_r)] \tag{2. 20}$$

where $K = 2\pi/\Lambda$ is the wave number of the wave pattern and $k = \frac{2\pi}{\lambda}$ is the wave number of the optical beam. The first-order intensity is normalized by the reflected specular beam prior to reaction. The normalized coefficient $C_0$ is the order of unity.

## 2.4 Metal/Semiconductor Contact

When a metal is making a contact with a semiconductor, a barrier will be formed at the metal-semiconductor interface [ 35]. This barrier can be either rectifying or nonrectifying. Schottky suggested that rectifying behavior could arise from a potential barrier generated as an effect of stable charges in the semiconductor. Then current can flow easily only in one directional very little in the other direction. This model is known as the Schottky barrier. On the other hand, ohmic contact is nonrectifying; that is to say, there is a little resistance to the current flow in the either direction.

When a metal makes a contact with a semiconductor two things happen. First, the Fermi levels in the two materials must be equal at thermal equilibrium. Second, the vacuum level must be continuous [26]. These two requirements ultimately determine the energy band diagram of the metal-semiconductor contact. **Figure2.4** shows the energy-band diagrams of metal-semiconductor contacts.

The barrier height $q\phi_{Bn}$ (for a n-type semiconductor) is the difference between metal work function and the electron affinity of the semiconductor :

$$q\phi_{Bn} = q(\phi_m - \chi)$$

On the other hand, the barrier height for a contact between a metal and semiconductor is :

$q\phi_{Bp} = Eg - q(\phi_m - \chi)$. Here Eg is the bandgap of the semiconductor; $q\phi_m$ is the work function of the metal, defined as the energy difference between the Fermi level and vacuum level ;

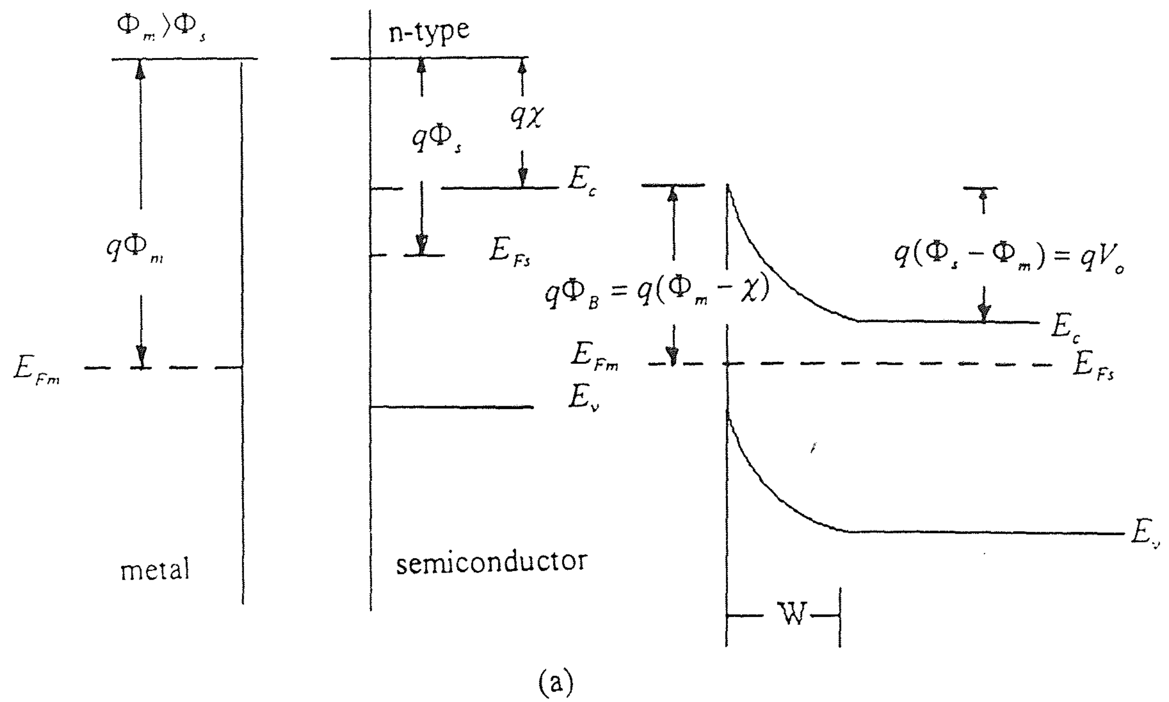


(a)

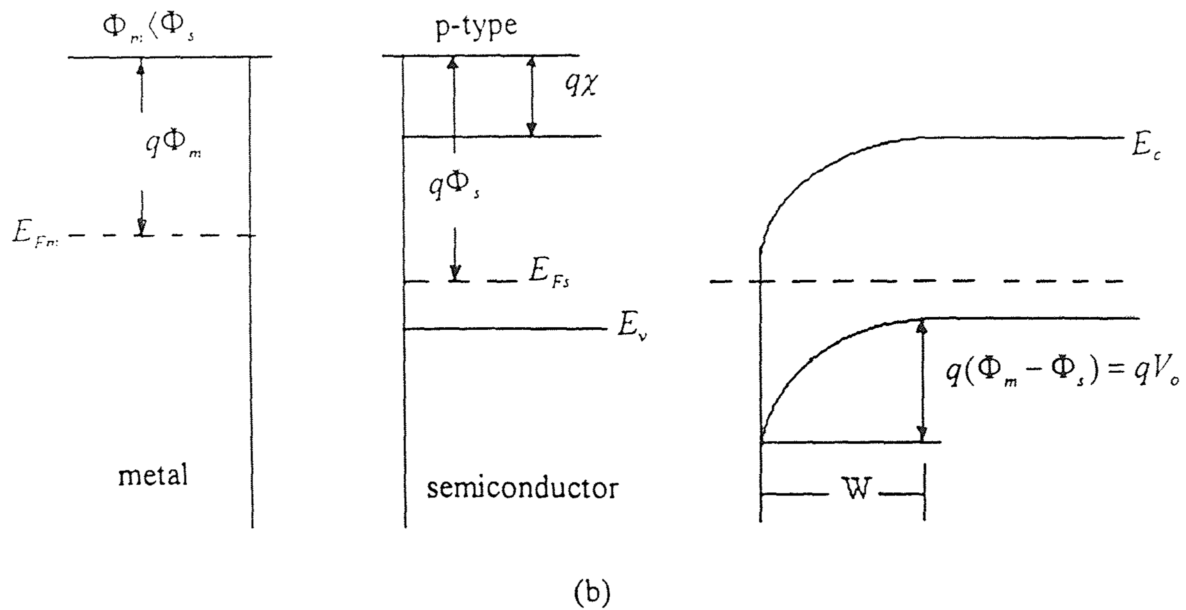


(b)

**Figure 2.4** The formation of a Schottky barrier between (a) n-type semiconductor with a metal with a larger work function; (b) p-type semiconductor and a metal having a smaller work function.

$q\chi$ is the electron affinity, defined as the energy difference between the conduction band edge and the vacuum level in the semiconductor, schematically shown in **Figure 2.4** Therefore, for a given semiconductor and for any metal, the sum of the barrier heights on n-type and p-type substrates is expected to be equal to the bandgap :

$$E_g = q(\phi_{Bn} + \phi_{Bp})$$

# CHAPTER 3

# EXPERIMENTS

## 3.1 System Set-up for Laser-Aided Interaction with Silicon Surface

### 3.1.1 System Set-up

The system for laser ablation and laser- induced chemical etching involves the set-up of an excimer laser as an etching beam, and a He-Ne laser as a secondary, background light source. The set up is shown schematically in **Figure 3.1.** The UV-light ( $\lambda$=248 nm, power of about 0.25 W at a repetition rate of 10 Hz ) from the excimer laser first passes through a focusing system composing of two cylindrical lenses which account to each excimer laser beam axis. Then the laser light passes through a collimating spherical lens and focusing cylindrical lens which finally translates the laser light to fall as a line on the sample. The sample is put on a stage capable of moving back and forth, up or down. The laser light can be incident perpendicularly or obliquely with respect to the surface of the substrate. The back and forth movement of the translational stage can be controlled both manually and automatically, whereas the up and down movement is done manually. The vertical movement is not done as often once the image of the line has been focused. The set up for the secondary light source is also shown in the **Figure 3.1**. The light from the He-Ne laser passes through a neutral filter and then incident on a sample by the use of a mirror. The circular neutral density filter controls the power of the He-Ne laser incident on the sample. The variation of power is linearly related to the angular position of the meter with respect to the incident beam. By moving the translation stage sequentially, a periodic grating structure is obtained by the etching process induced by the excimer laser beam.

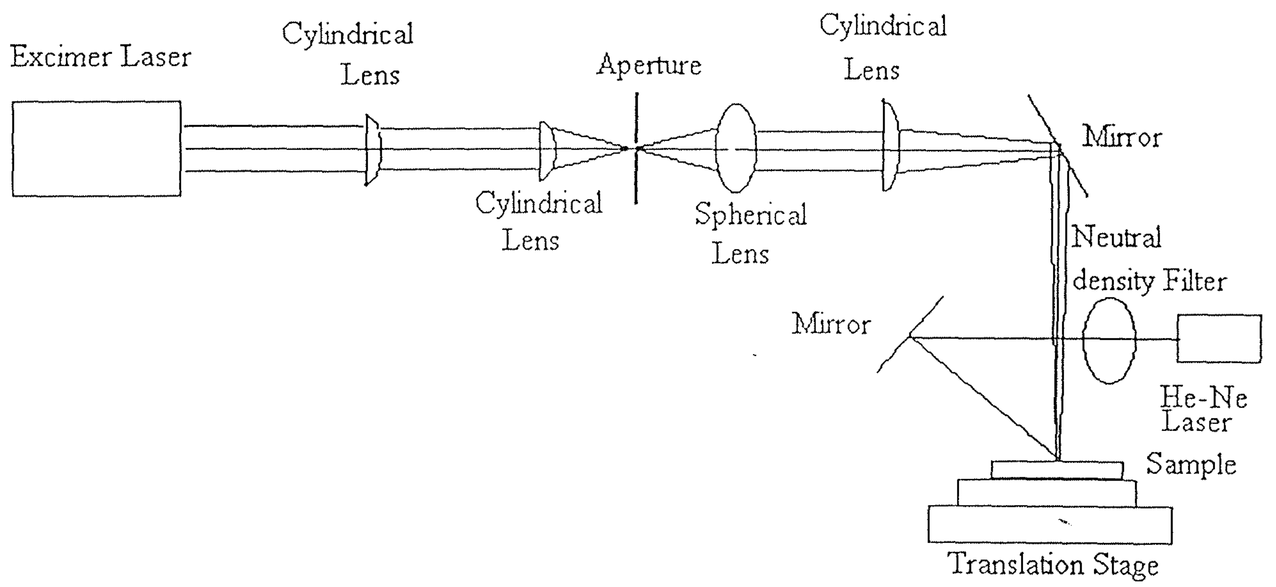


**Figure 3.1** Schematic showing the system set-up for laser-induced patterning.

The set up for optically monitoring the grating profile is shown in **Figure 3.2.** A monitoring He-Ne laser light which is allowed to incident on the grating and the intensities of the diffracted beams are then measured. The profile is calculated based on the intensity of the diffraction modes.

### 3.1.2. The Laser System

The lasers that have been used in our experiments are KrF excimer laser and He-Ne helium-neon laser. The KrF excimer laser (Lamda Physik EMG 102 MSC) has been used as an etching system with a wavelength of 248 nm, pulse duration of about 10 ns, and average output power of 0.25 W at a repetition rate of 10 Hz. The main advantages of this type of a pulsed-laser is its high power favorable for rapid and high material removal rate that have already been discussed. The disadvantages that are generally encountered are: damages of the substrate surface structure, and appearances of the ripple pattern. The main limitation, though, of the excimer laser is the difficulty involved in focusing due to its relatively poor coherence; the output of an excimer laser is highly multimodal and contains as many as $10^5$ transverse modes.

Helium-neon laser was used as a secondary light source and was also used as a probe beam to measure the grating depth profile. The He-Ne was a continuous wave (CW) laser. It was operated at a power level of about 5 mW.

## 3.2 Material Preparation

### 3.2.1. Surface Treatment

Single crystal wafers of both n-type and p-type silicon(100) were used in the experiments. The dopant concentration was approximately $10^{16}$ /cm$^3$. Both the

surfaces of the wafers mirror-polished by a chemico-mechanical method, so that no further treatment of this type was necessary.

Contamination of the surface is not desirable. The surface of the specimen was treated before the laser processing. Some experiments though were performed without passivating the silicon surfaces with hydrofluoric acid. We have found that similar results have been obtained for treated and non treated Si samples. In our experiments, the following steps were used to create a flat and damage-free surface:

1. Polish in Bromine-methanol ( $Br_2$ : $CH_3OH$ = 1: 99 by vol. ) for 1 minute.
2. Rinse with methanol for 30 seconds.
3. Wash in distilled, de ionized water for 30 seconds.
4. Etch in dilute hydrofluoric acid ( HF (48%) : $H_20$ = 1: 9 by vol. ) for 30 seconds.
5. Wash in deionized water for 30 seconds.
6. Air blow-dry immediately.

### 3.2.2. Electrolytes

The concentration of the electrolyte is an important parameter in determining the etching rate. Two typical electrolytes were used. One is orientation-dependent etchant, KOH : $H_2O$, with a ratio of 1 : 20 by volume. The other is a solution of HF : $HNO_3$ : $H_2O$ with a volume ratio of 2 :3 :100. Both aqueous solutions were of sufficient dilution to cause little or no dark etching were present. The irradiation with the ultraviolet laser might increase the temperature of the substrate. However, no modest increase in temperature has been observed . So, the solution was at normal room temperature.

## 3.3. Laser Ablation

### 3.3.1. Laser Ablation in Air

A set of experiments was carried out to generate a pattern on silicon surfaces by focusing an excimer laser beam . Both n-type and p-type silicon(100) were used to demonstrate the laser ablation in air. In order to get high aspect ratio features, the laser beam was focused on the surface of the substrate by carefully adjusting the position of the sample. Periodic pattering has been achieved by moving the substrate sequentially in a perpendicular direction to the etching line profile, one step at a time. The depth profiles were generated by varying the number of pulses of an excimer laser. A separate set of experiments was also carried out by using the He-Ne laser simultaneously with the excimer laser to demonstrate its effect as a background light source on the etching rate.

### 3.3.2 Thin-Film Cell Configuration

A small quantity of the electrolyte solution was dropped on a treated specimen surface by a neutralization pipette. A quartz cover plate ( 22 mm × 22 mm × 0.18 mm) was then put on the specimen and was held by capillary action. Quartz was used as a cover glass because of its low absorption coefficient in the wavelength of the ablating laser. The cell was then patterned under the illumination of the focused laser beam. The configuration, which is also called a thin-film cell configuration is shown in **Figure 3.3.**

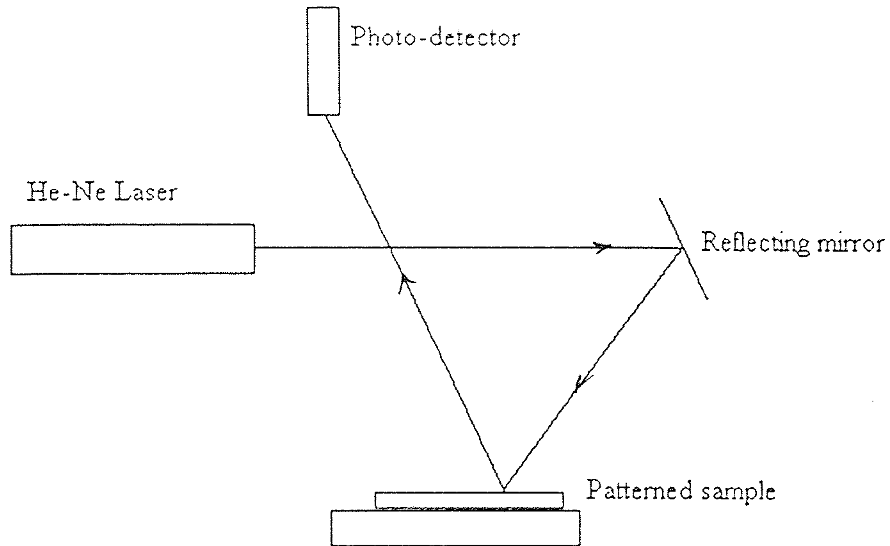


**Figure 3.2** Schematic showing arrangements for the diffraction mode measurement.

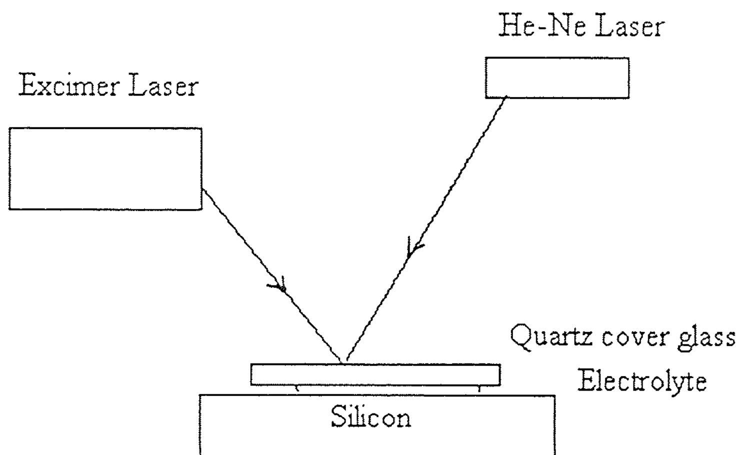


**Figure 3.3** Schematic showing the PEC thin-film cell configuration.

## 3.4. Measurement of Groove Profiles

### 3.4.1. Techniques for the Measurements

Four methods were used to monitor the profile of the surface patterns. These were: the alpha-step recorder measurement, optical microscopy, diffraction modes measurements, and scanning electron microscopy.

In the early stage of our experiments, we tried to measure the groove configurations by an optical microscope and by an alpha-step recorder. We found both of them incapable to measure the profile appropriately. The magnification and resolution attained by the optical microscope was too low for the real effect to be detected. In case of the alpha-step recorder, we found the tip of the needle that runs across the patterned surface to measure the profile depth was too big. We finally chose the electron microscopy technique as well as light diffraction measurement technique to measure the pattern depth profile.

### 3.4.1 Diffraction Modes Measurement

We measured all of the diffraction mode intensity and calculated the grating depth by Fourier Analysis explained in section 2.2.4. The arrangement of the diffraction mode measurement is shown in **Figure 3.2.** A weak probe beam of He-Ne with wavelength 633 nm was used as a incident light source. The intensity of the diffracted light from the flat, clean, and unetched surface, $I_{00}$, was measured first to normalize the diffraction modes of the etched grating. The incident angle was chosen as $\phi_i$. The measuring plane was a perpendicular surface with a distance d from the sample. The distance between each two diffraction modes was also measured. The photo detector was placed on a 3-D translator to adjust the position of the each mode.

## 3.5 Metal-Semiconductor Contact Preparation

Aluminum was deposited on silicon surface to form a Schottky-barrier contact. The ohmic contact was prepared by putting aluminum on the back side of the wafer followed by laser annealing. They were cleaned before any contact was prepared :

1. Clean in acetone for 5 minutes.
2. Wash in deionized water for 30 seconds.
3. Heat ( 800 C) in 10 % HCl for 10 minutes.
4. Wash in deionized water for 30 seconds.
5. Etch in dilute hydrofluoric acid ( 5 % vol. HF ) for 1 minute.
6. Wash in deionized water
7. Air-blow-dry immediately.

### 3.5.1. Schottky-Barrier and Ohmic Contact

The Schottky- contact was generated between aluminum and p-type silicon (100) wafer, while the ohmic contact was made between aluminum and back side of the silicon wafer followed by the laser treatment. The evaporation of Al was done in a high vacuum system. The evaporation pressure was 2 * 10 E-5 torr. When each deposition was completed, the samples were cooled down to room temperature in the vacuum chamber to prevent oxidation. The laser annealing was done on the back side of the wafer after the metal (aluminum) was deposited in order to get an ohmic contact by reducing the barrier height.

### 3.5.2. Barrier Height Measurement of Metal/Semiconductor Contact

In our experiment we used the current-voltage technique to determine the barrier height of metal-semiconductor contact. Because the current-voltage characteristics are widely used to determine the saturation current (Is), the threshold voltage (Vth)

and the Schottky barrier height (SBH) [23] The barrier height is most commonly calculated from the saturation current (Is) which is determined by extrapolating the forward I-V characteristics to zero applied voltage. The current axis intercept for the straight line portion of the semi-log plot at V= 0 is given by Is. The barrier height $\phi_B$ is calculated according to [36]

$$\phi_B = \frac{kT}{q} In(\frac{AA^{**}}{I_S} T^2)$$

The barrier height so determined is $\phi_B$ for zero bias. Where as saturation current Is is given by : [36]

$$Is = AA^{**} T^2 \exp(-q\phi_B / kT)$$

Where A** is the Richardson's Constant. Its value for silicon is 120 A /cm$^2$ K$^2$.

# CHAPTER 4

# EXPERIMENTAL RESULTS

## 4.1 The Grating Groove Profiles

### 4.1.1. The Grating Profile Due to Ablation in Air

The surface patterning induced on silicon surfaces were fabricated with the system set-up shown in **Figure 3.1**. The depth and periodicity of the grating profiles of silicon surfaces were largely measured by a scanning electron microscope (SEM). The first-order light diffraction intensity measurement technique was used to verify the findings obtained by the SEM.

**Figures 4.1 to 4.3** show the scanning electron micrographs of the groove profiles of a n-type Si (100) ablated with the KrF laser ( $\lambda$ = 248 nm ) with different number of pulses in air with a laser power of 0.25 watt at a repetition rate of 10 Hz. The silicon was used in as is condition for these experiments. **Figure 4.4** shows the groove depth vs. the number of pulses of the incident excimer laser beam on n-type silicon (100) surfaces.

**Figures 4.5 to 4.7** show the scanning electron micrographs of the groove profiles of p-type Si (100) ablated with the KrF laser ( $\lambda$ = 248 nm ) under different number of pulses in air with a laser power of 0.25 watt on a repetition rate of 10 Hz. The silicon was used in as is condition for these experiments. **Figure 4.8**shows the groove depth vs. the number of pulses of the incident excimer laser beam on p-type silicon (100) surfaces.

**Figures 4.9 to 4.11** show the scanning electron micrographs of the groove profiles of p-type Si (100) ablated with the KrF laser ( $\lambda$ = 248 nm ) with different numbers of pulses in air with a laser power of 0.25 watt at a repetition rate of 10 Hz in presence of background illumination of He-Ne laser ( $\lambda$= 633 nm) with a

power of 5 mW. The silicon used in the experiments was in an as is condition. **Figure 4.12** shows the depth profile of the grooves vs. the number of pulses of the incident excimer laser beam on a p-type silicon in presence of a secondary light of a 5 mW He-Ne ( $\lambda = 633$ nm) laser with a power of 5 mW.

**Figures 4.13 to 4.17** show the scanning electron micrographs of the groove profiles of n-type Si (100) ablated with the KrF laser ( $\lambda = 248$ nm ) with different numbers of pulses in air with a laser power of 0.25 watt at a repetition rate of 10 Hz. The silicon was treated described in the section 3.2.1 for these experiments. **Figure 4.18** shows the groove depth vs. the number of pulses of the incident excimer laser beam on n-type silicon (100) surfaces.

### 4.1.2. The Grating Profile Due to Wet Chemical Etching

**Figures 4.19 to 4.23** show the scanning electron micrographs of the groove profiles of p-type Si (100) etched with the KrF laser ( $\lambda = 248$ nm ) in KOH : $H_2O$ = 1 : 20 solution. The laser power was 0.25 watt on a repetition rate of 10 Hz in presence of different background illuminations ( i.e., 0, 1.25, 2.50, 3.75, and 5 watts respectively). The patterns were engraved on the silicon with 30 laser pulses. For the wet chemical-etching the same experimental set up as **Figure 3.1** was used. In addition, a liquid-phase thin-film cell configuration was made. **Figure 4.24** shows the groove depth vs. the intensity of background illuminations for a p-type Si (100)/KOH : $H_2O$ system.

**Figures 4.25 to 4.29** show the scanning electron micrographs of the groove profiles of n-type Si (100) etched with the KrF laser ( $\lambda = 248$ nm ) in KOH : $H_2O$ = 1 : 20 solution. The laser power was 0.25 watt at a repetition rate of 10 Hz in the presence of different background illuminations ( i.e., 0, 1.25, 2.50, 3.75, and 5 watts respectively). The patterns were engraved on the silicon surface with 30 pulses of

the excimer laser irradiated on the surfaces. For the wet chemical-etching the same experimental set up was used. In addition to this, a liquid-phase thin-film cell configuration was made. **Figure 4.30** shows the groove depth vs. the intensity of background illuminations for the n-type Si (100)/KOH : $H_2O$ system.

**Figures 4.31 to 4.35** show the scanning electron micrographs of the groove profiles of p-type Si (100) etched with the KrF laser ( $\lambda$ = 248 nm ) in HF : $HNO_3$ : $H_2O$ = 2 : 3 : 100 solution. The laser power was 0.25 watt at a repetition rate of 10 Hz in presence of different background illuminations ( i.e., 0, 1.25, 2.50, 3.75, and 5 watts). The patterns were engraved on the silicon surface with 30 pulses of the excimer laser irradiated on the surfaces. For the wet chemical-etching the same set up (as shown in the **Figure 3.1**) was used. In addition to this, a liquid-phase thin-film cell configuration was made. **Figure 4.36** shows the groove depth vs. the intensity of background illuminations for the p-type Si (100)/ HF: $HNO_3$ : $H_2O$ system. The silicon surfaces were used in the 'as it is' condition.

**Figures 4.37 to 4.40** show the scanning electron micrographs of the groove profiles of n-type Si (100) etched with the KrF laser ( $\lambda$ = 248 nm ) in KOH: $H_2O$ = 1 : 20 solution. The laser power was 0.25 watt at a repetition rate of 10 Hz in presence of different background illuminations ( i.e., 0, 1.25, 3.75, and 5 watts). The patterns were engraved on the silicon with 20 pulses of the excimer laser irradiated on the surfaces. For the wet chemical-etching the same set up (as shown in the **Figure 3.1**) was used. In addition to this, a liquid-phase thin-film cell configuration was made. **Figure 4.41** shows the groove depth vs. the intensity of background illuminations for the n-type Si (100)/ KOH : $H_2O$ system. The silicon surfaces were used in the as it is condition.

### 4.2 Grating Depth Evaluation by Diffraction Measurement Technique

The results of the measurements of the grating profiles by use of first-order light diffraction intensity measurement technique are presented here. The detail of the measurement technique has been presented in the section 3.4.1. **Tables 4.1 to 4.5** represent the data obtained from the sample numbers 1 to 10. The measured diffraction modes have been presented as intensity measurement data.

**Table 4.1** represents the data for samples 1 and 2 fabricated by only 1 pulse of the excimer laser per groove for p-type Si (100)/KOH : $H_2O$ system without any background light. **Table 4.2** represents the data for samples 3 and 4 fabricated by only 1 pulse per groove by the excimer laser for p-type Si (100)/KOH : $H_2O$ system with a background light of 1.25 mW. **Table 4.3** represents the data for samples 5 and 6 fabricated by only 1 pulse per groove by the excimer laser for p-type Si (100)/KOH : $H_2O$ system with a background light of 2.5 mW. **Table 4.4** represents the data for samples 7 and 8 fabricated by only 1 pulse per groove by the excimer laser for p-type Si (100)/KOH : $H_2O$ system with a background light of 3.75 mW. **Table 4.5** represents the data for samples 9 and 10 fabricated by only 1 pulse per groove by the excimer laser for p-type Si (100)/KOH : $H_2O$ system with a background light of 5 mW.

**Fig. 4.42** shows the grating groove depth vs. the total background light for the p-type Si(100)/ KOH : $H_2O$ system. Only 1 pulse per groove was used to induce the pattern. The groove depth was measured by the light diffraction intensity measurement technique as described in section 3.4.1.

### 4.2.1. The Analysis of Grating Profile

The theory of the grating profile was discussed in section 2.3. The real grating profile can be found by assuming :

1. The pattern and intensity of the diffraction modes are symmetrical, meaning $I_{-1} = I_{+1}$, $I_{-2} = I_{+2}$ and so on.
2. The signs of the phases are chosen in accordance to the sign of the appropriate of the Bessels functions.
3. The depth of the etching profile can be found out using the Eq. 2.11.

## 4.3 Barrier Height Measurement

The method of determination of the barrier height was presented in section 3.5.2. Here the results of the calculations for barrier heights for metal-semiconductor contacts will be presented. **Table 4.6** shows all the calculated barrier heights accompanied by their corresponding junction areas and saturation currents both on the pattered and flat surfaces, the depth and periodicity of the patterns on which the metal-semiconductor contacts were made.

**Figures 4.43 to 4.47** show the forward current-voltage ( I-V ) characteristics of Al /p-type Si (100) contacts both on patterned and flat surfaces. **Figure 4.43** shows the I-V characteristics for the Al /P-type Si (100) contacts both on the patterned ( periodicity ≈ 15μm and depth □≈ 15 nm ) and flat surfaces. Contact areas for flat and patterned areas are $3.14 \times 10^{-2}$ and $4.14 \times 10^{-2}$ $cm^2$ respectively of the sample number 1.

**Figure 4.44** shows the I-V characteristics for the Al /P-type Si (100) contacts both on the patterned ( periodicity ≈ 15μm and depth □≈ 25 nm ) and flat surfaces.

Contact areas for flat and patterned areas are $3.14 \times 10^{-2}$ and $4.14 \times 10^{-2}$ $cm^2$ respectively for the sample number 2.

**Figure 4.45** shows the I-V characteristics for the Al /P-type Si (100) contacts both on the patterned ( periodicity ≈ 125µm and depth □≈ 5 µm ) and flat surfaces. Contact areas for both the cases are $0.7854 \times 10^{-2}$ $cm^2$ for the sample number 3.

**Figure 4.46** shows the I-V characteristics for the Al /P-type Si (100) contacts both on the patterned ( periodicity ≈ 250 µm and depth □≈ 5 µm ) and flat surfaces. Contact areas for both the cases are $0.7854 \times 10^{-2}$ $cm^2$ for the sample number 4.

**Figure 4.47** shows the I-V characteristics for the Al /P-type Si (100) contacts both on the patterned ( periodicity ≈ 375 µm and depth □≈ 5 µm ) and flat surfaces. Contact areas for both the cases are $3.14 \times 10^{-2}$ $cm^2$ for the sample number 5.

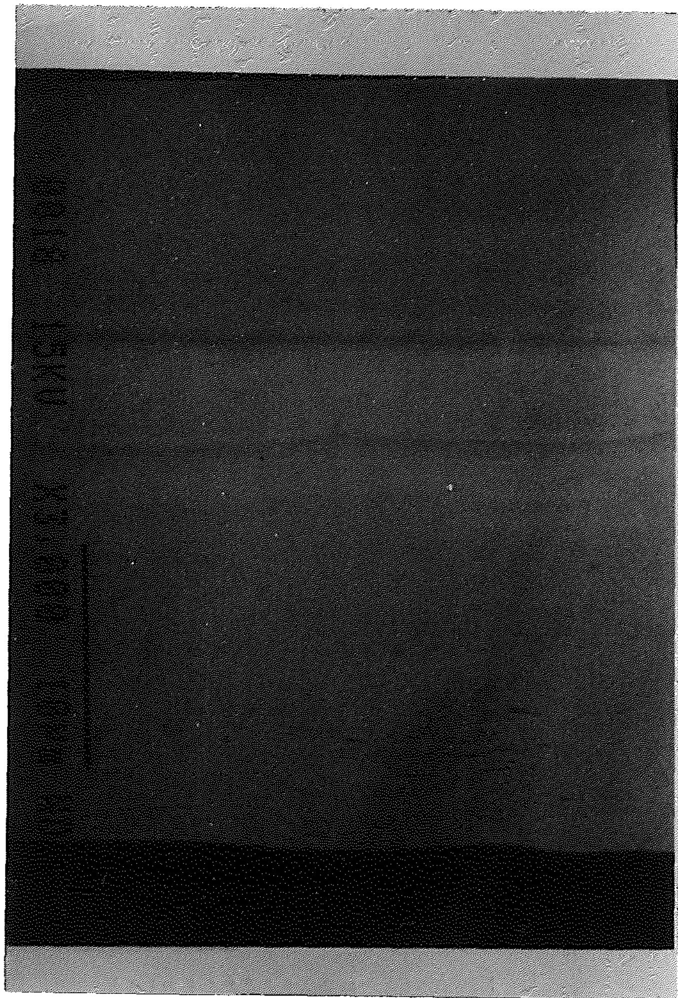

**Figure 4.1** Scanning electron micrograph showing the groove profile of a n-type Si(100) surface ablated with the KrF laser ( λ =248 nm) beam in air. [ 10 pulses per groove were used to induce this pattern].

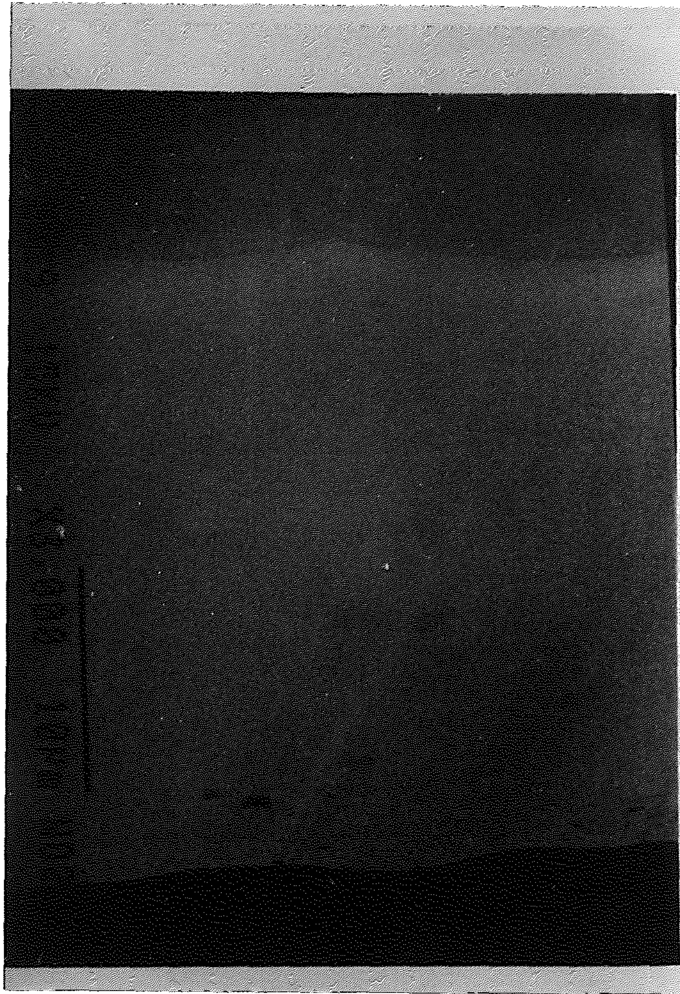

**Figure 4.2** Scanning electron micrograph showing the groove profile of a n-type Si(100) surface ablated with the KrF laser ( λ =248 nm) beam in air. [ 20 pulses per groove were used to induce this pattern].

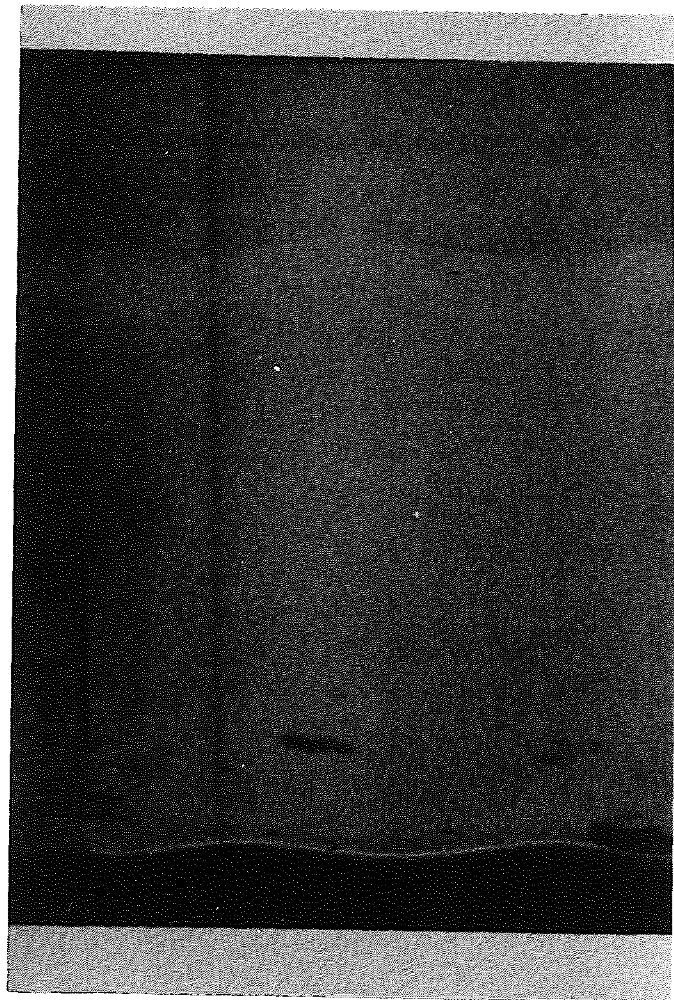

**Figure 4.3** Scanning electron micrograph showing the groove profile of a n-type Si(100) surface ablated with the KrF laser ( $\lambda$ =248 nm) beam in air. [ 30 pulses per groove were used to induce this pattern].

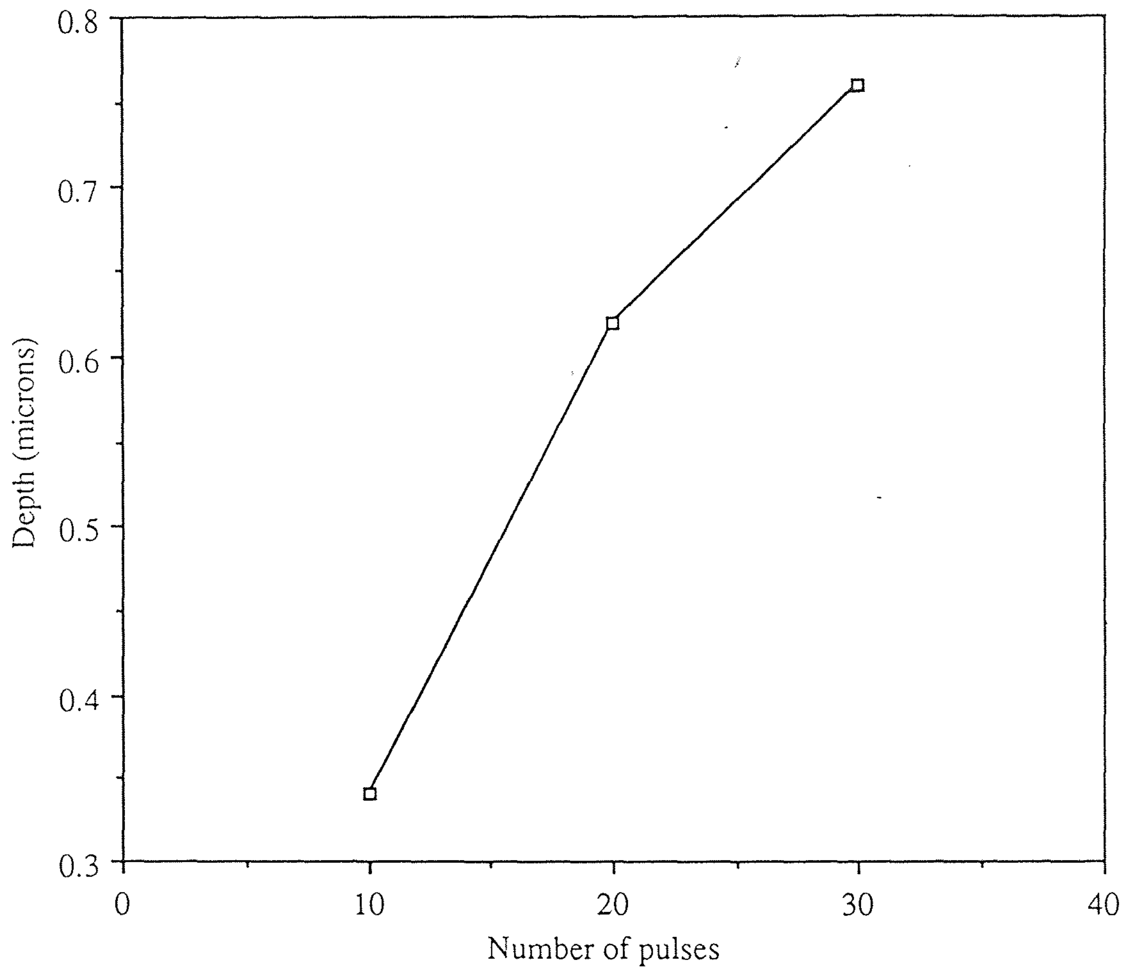


**Figure 4.4** The grating depth profile versus the number of pulses of the incident excimer laser ($\lambda$ =248 nm) beam on a n-type Si (100) surface.[ The points were evaluated by SEM measurements].

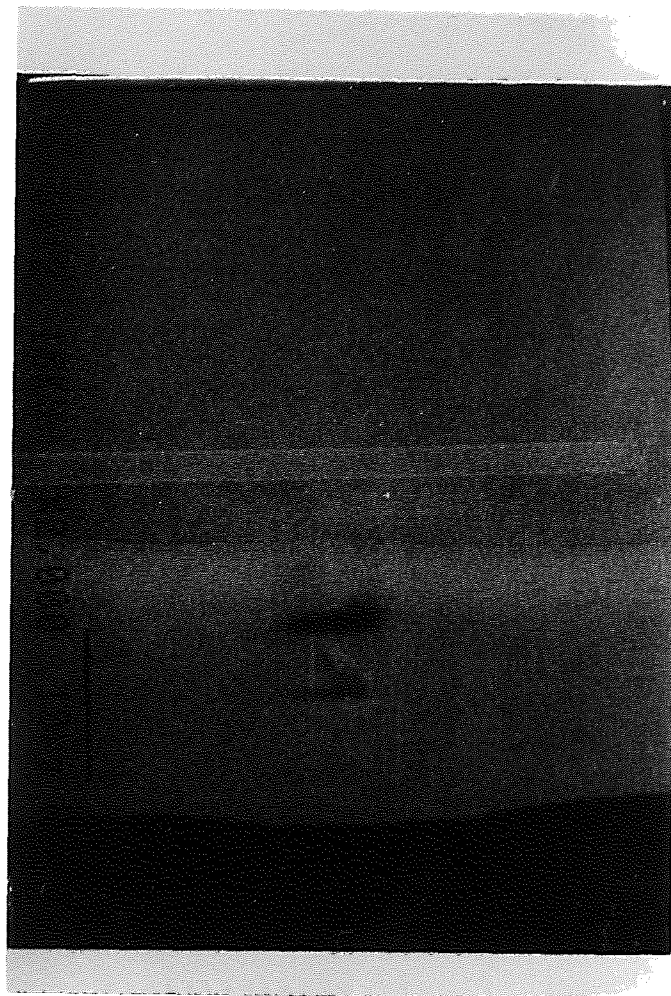

**Figure 4.5** Scanning electron micrograph showing the groove profile of a p-type Si(100) surface ablated with the KrF laser ( $\lambda$ =248 nm) beam in air. [ 10 pulses per groove were used to induce this pattern].

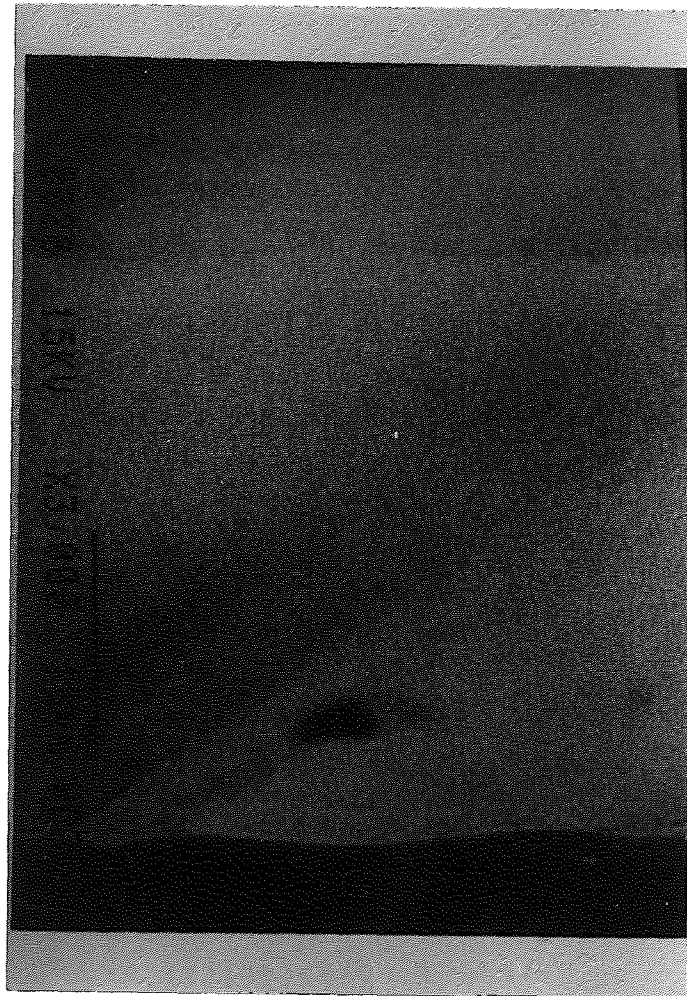

**Figure 4.6** Scanning electron micrograph showing the groove profile of a p-type Si(100) surface ablated with the KrF laser ( $\lambda$ =248 nm) beam in air. [ 20 pulses per groove were used to induce this pattern].

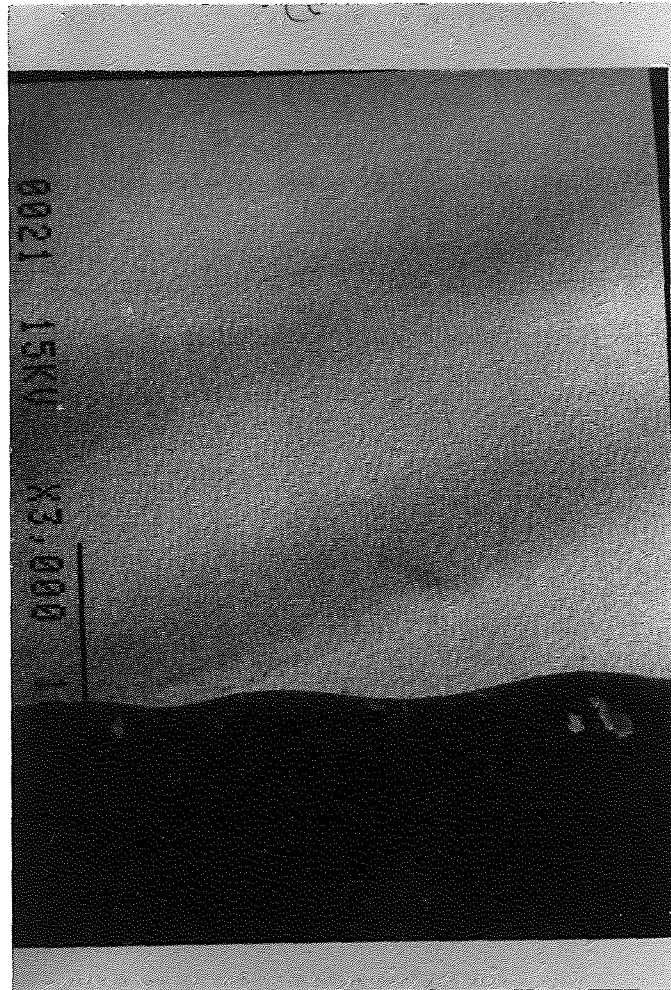


**Figure 4.7** Scanning electron micrograph showing the groove profile of a p-type Si(100) surface ablated with the KrF laser ( $\lambda$ =248 nm) beam in air. [ 30 pulses per groove were used to induce this pattern].

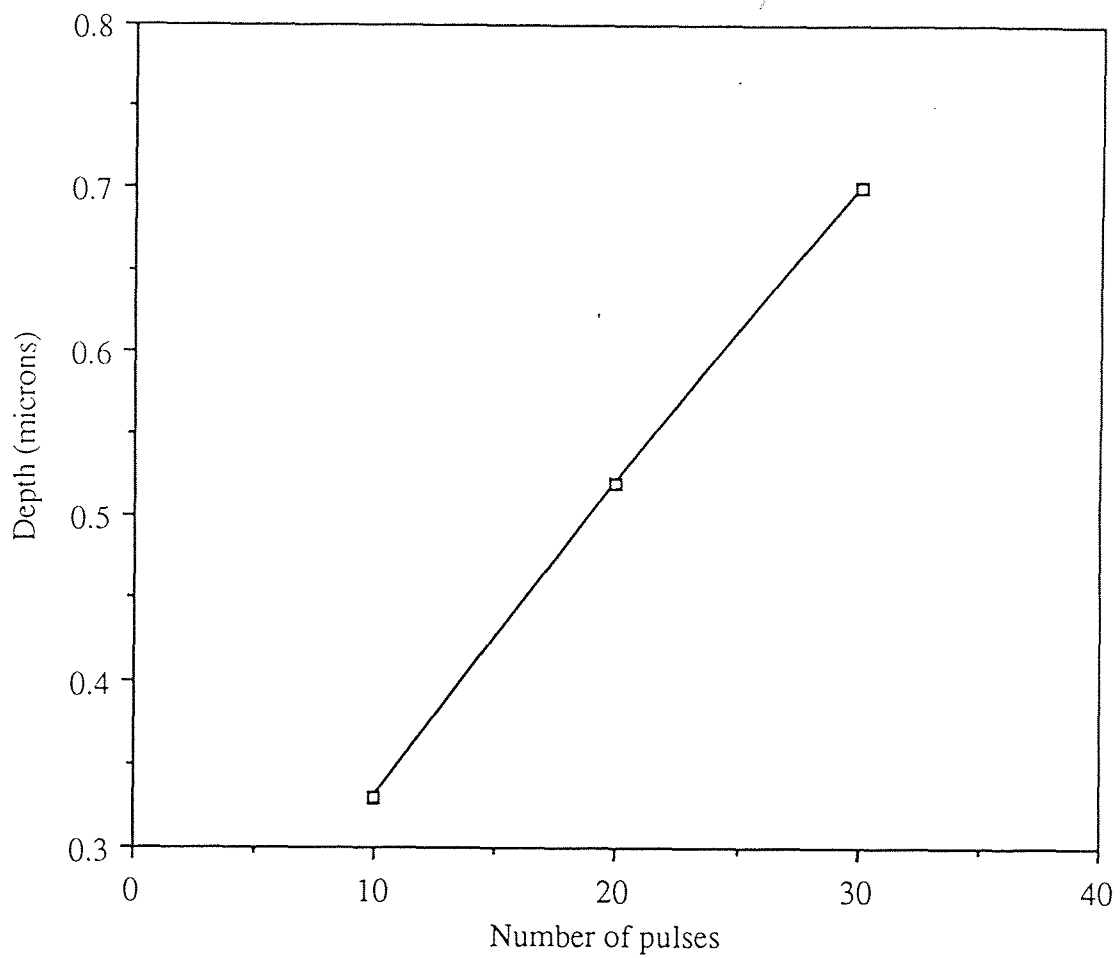


**Figure 4.8** The grating depth profile versus the number of pulses of the incident excimer laser ($\lambda$ =248 nm) beam irradiated on a p-type Si (100) surface in air.[ The points were evaluated by SEM measurements].

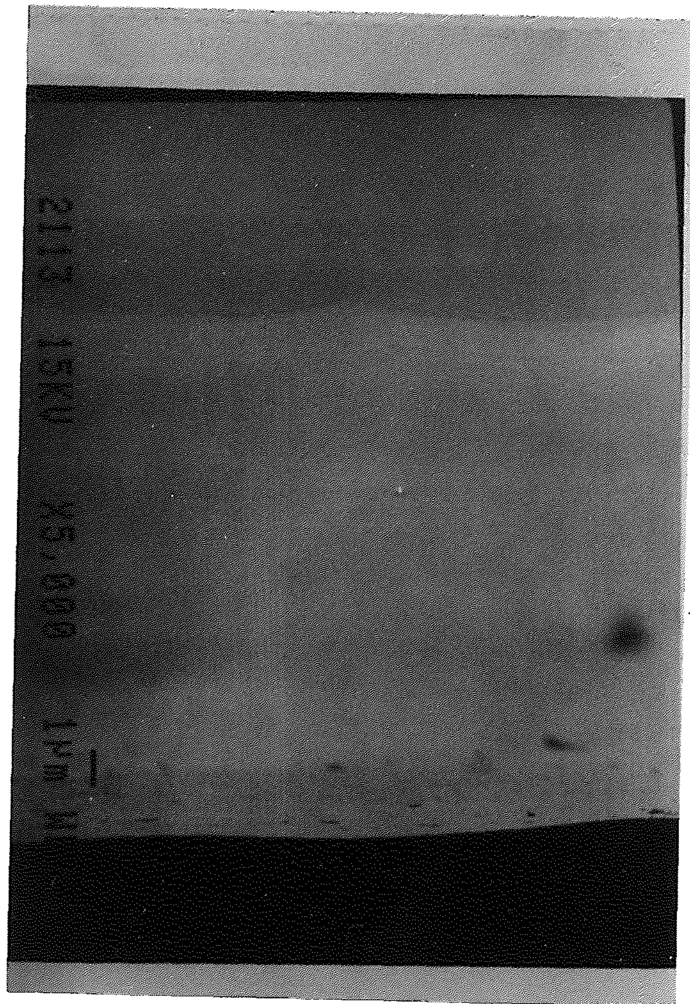


**Figure 4.9** Scanning electron micrograph showing the groove profile of a p-type Si(100) surface ablated with the KrF laser ( $\lambda$ = 248nm ) beam in air in presence of a background light source, HeNe laser ( $\lambda$= 633 nm). [ 10 pulses of the excimer laser beam per groove were used to induce this pattern).

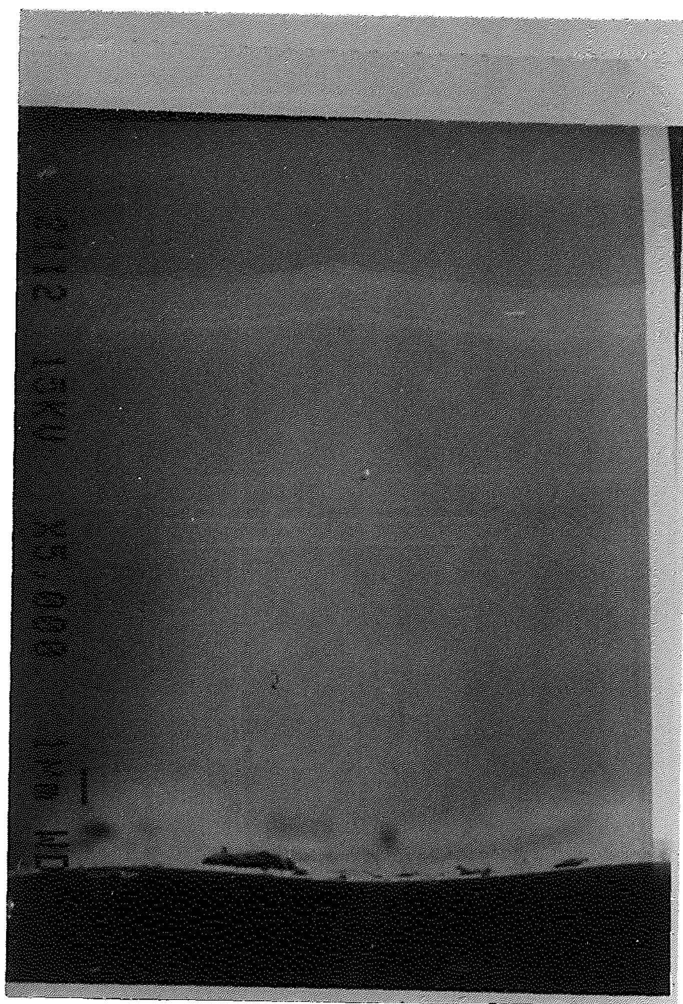

**Figure 4.10** Scanning electron micrograph showing the groove profile of a p-type Si(100) surface ablated with the KrF laser ( $\lambda$ = 248nm ) beam in air in presence of a background light source, HeNe laser ( $\lambda$= 633 nm). [ 20 pulses of the excimer laser beam per groove were used to do this pattern].

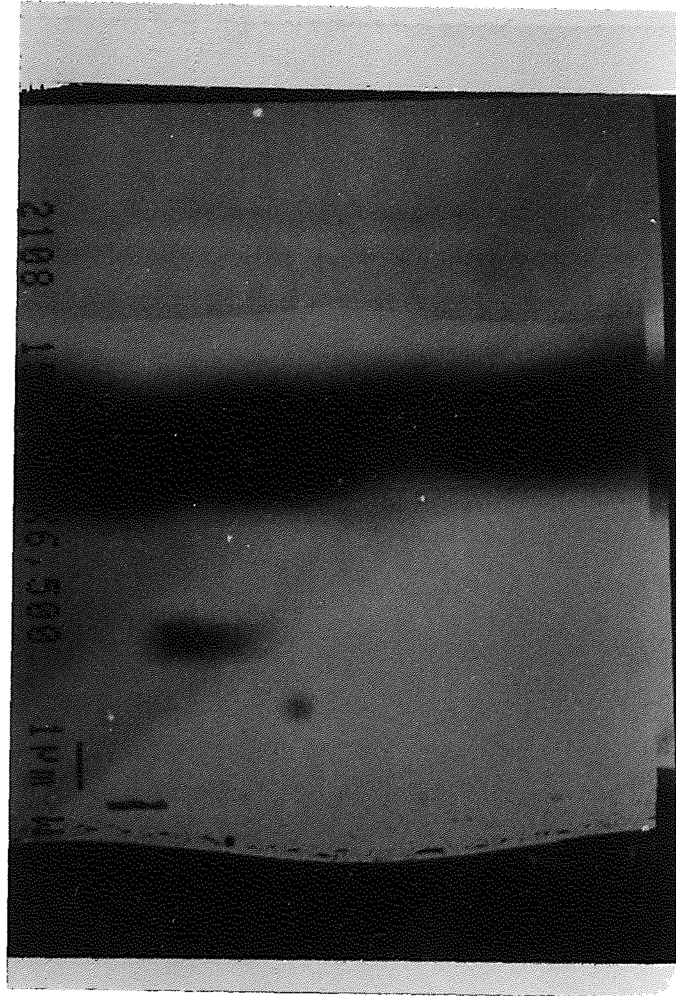


**Figure 4.11** Scanning electron micrograph showing the groove profile of a p-type Si(100) surface ablated with the KrF laser ( $\lambda$ = 248nm ) beam in air in presence of a background light source, HeNe laser ( $\lambda$= 633 nm). [ 30 pulses of the excimer laser beam per groove were used to do this pattern].

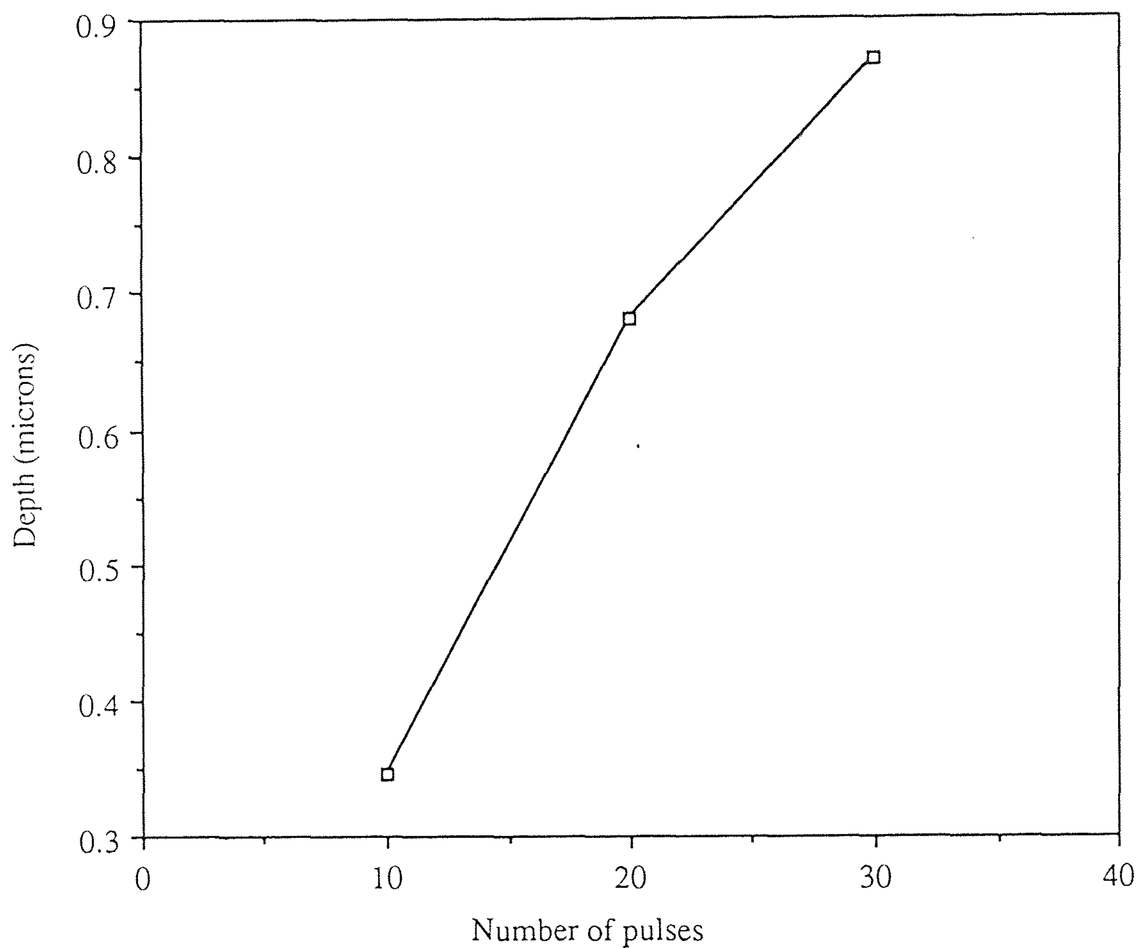


**Figure 4.12** The grating depth profile versus the number of pulses of the incident excimer laser (λ =248 nm) beam on irradiated on a p-type Si (100) surface in presence of a background light source, HeNe laser ( λ= 248 nm ) beam in air [ The points were evaluated by SEM measurements].

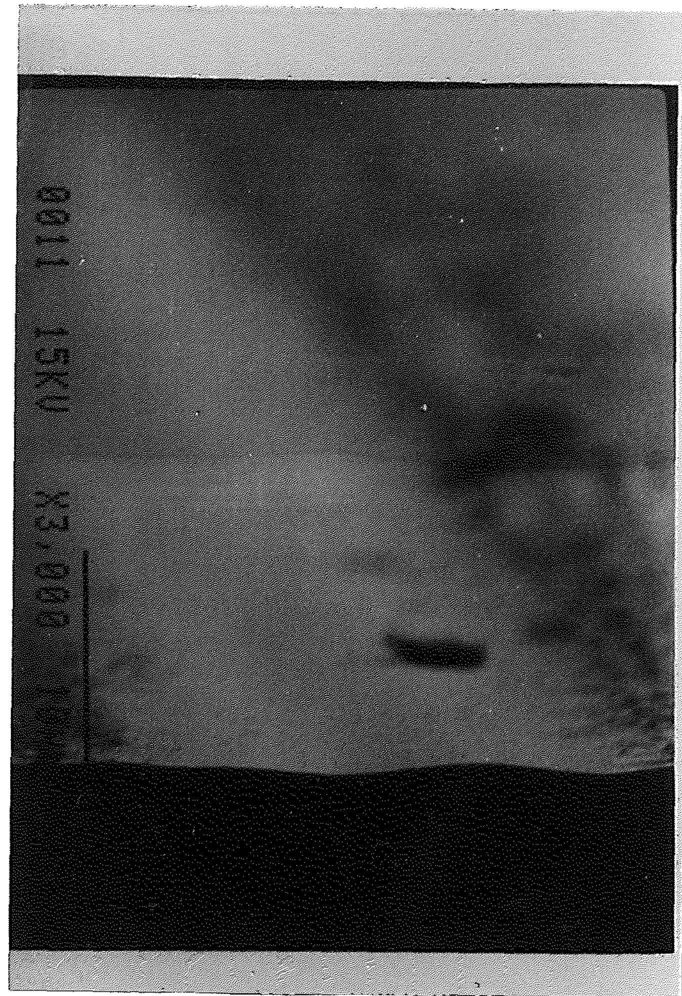


**Figure 4.13** Scanning electron micrograph showing the groove profile of a n-type Si(100) surface ablated with the KrF laser ( λ =248 nm ) beam in air. [ 50 pulses per groove were used to induce this pattern].

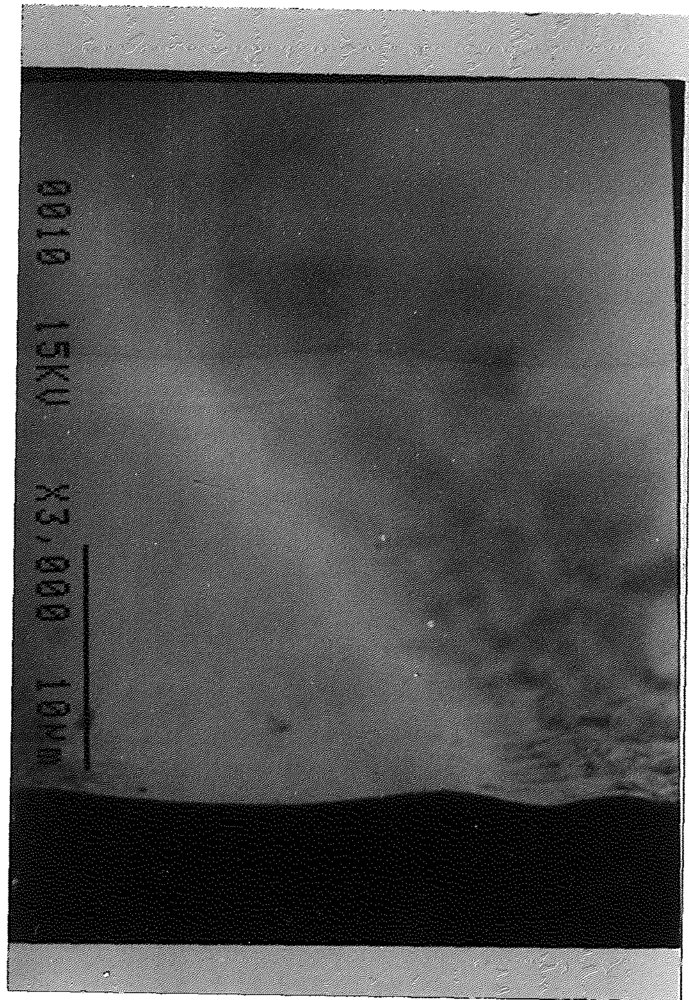


**Figure 4.14** Scanning electron micrograph showing the groove profile of a n-type Si(100) surface ablated with the KrF laser ( λ =248 nm ) beam in air. [100 pulses per groove were used to induce this pattern].

**Figure 4.15** Scanning electron micrograph showing the groove profile of a n-type Si(100) surface ablated with the KrF laser ( $\lambda$ =248 nm ) beam in air. [150 pulses per groove were used to induce this pattern].

**Figure 4.16** Scanning electron micrograph showing the groove profile of a n-type Si(100) surface ablated with the KrF laser ( λ =248 nm ) beam in air. [200 pulses per groove were used to create this pattern].

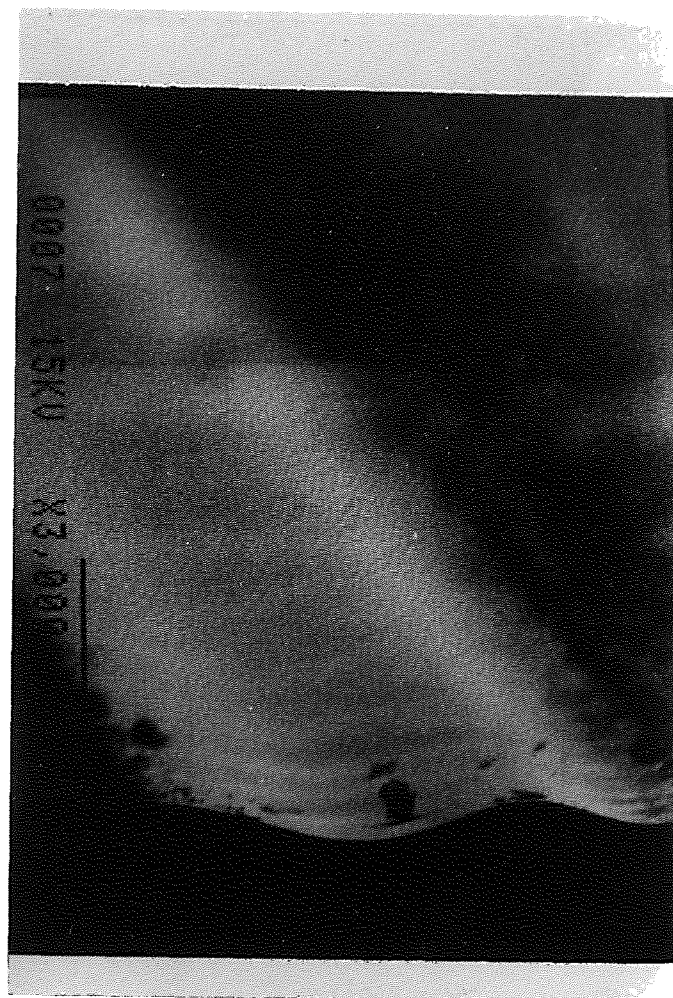


**Figure 4.17** Scanning electron micrograph showing the groove profile of a n-type Si(100) surface ablated with the KrF laser ( $\lambda$ =248 nm ) beam in air. [250 pulses per groove were used to create this pattern].

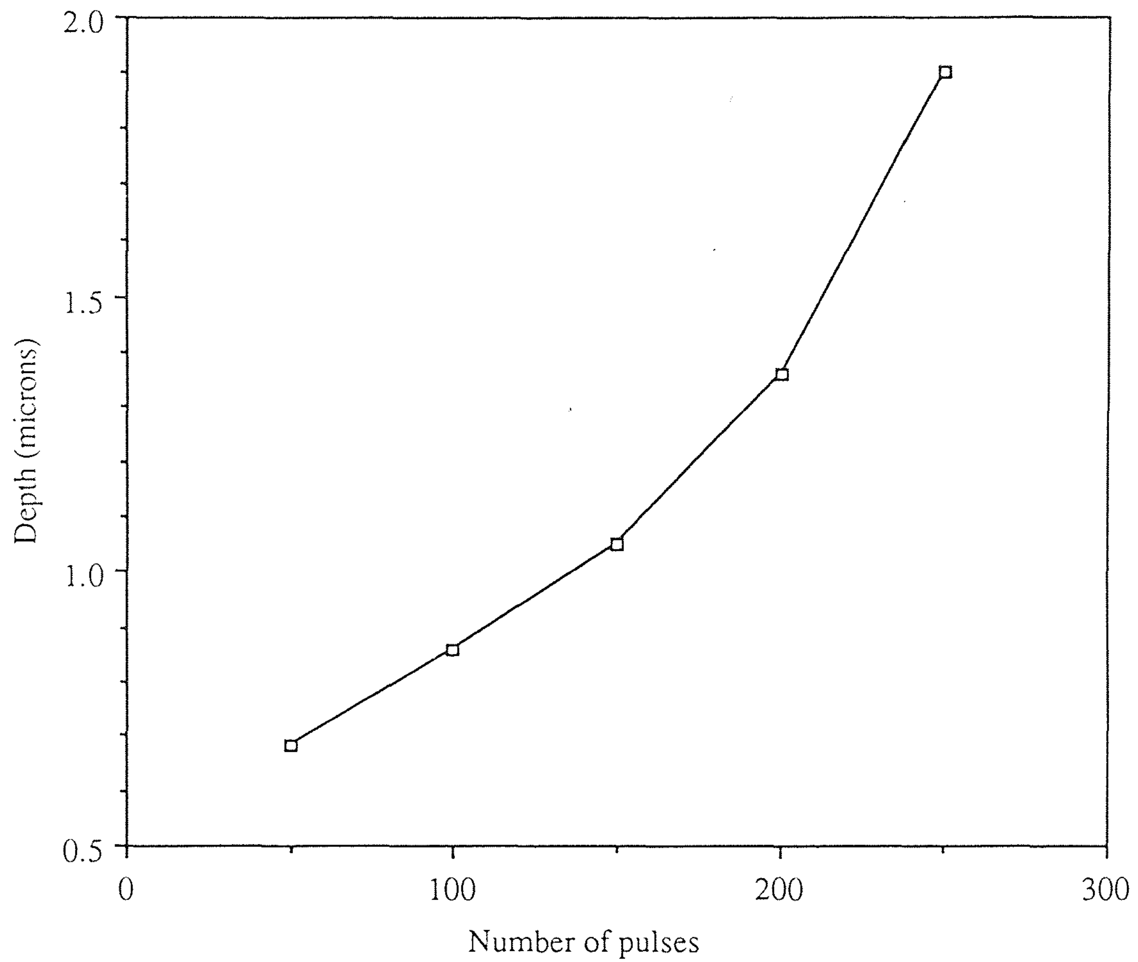


**Figure 4.18** The grating depth profile versus the number of pulses of the incident excimer laser ($\lambda$ =248 nm) beam on a n-type Si (100) surface.[ The points were evaluated by SEM measurements].

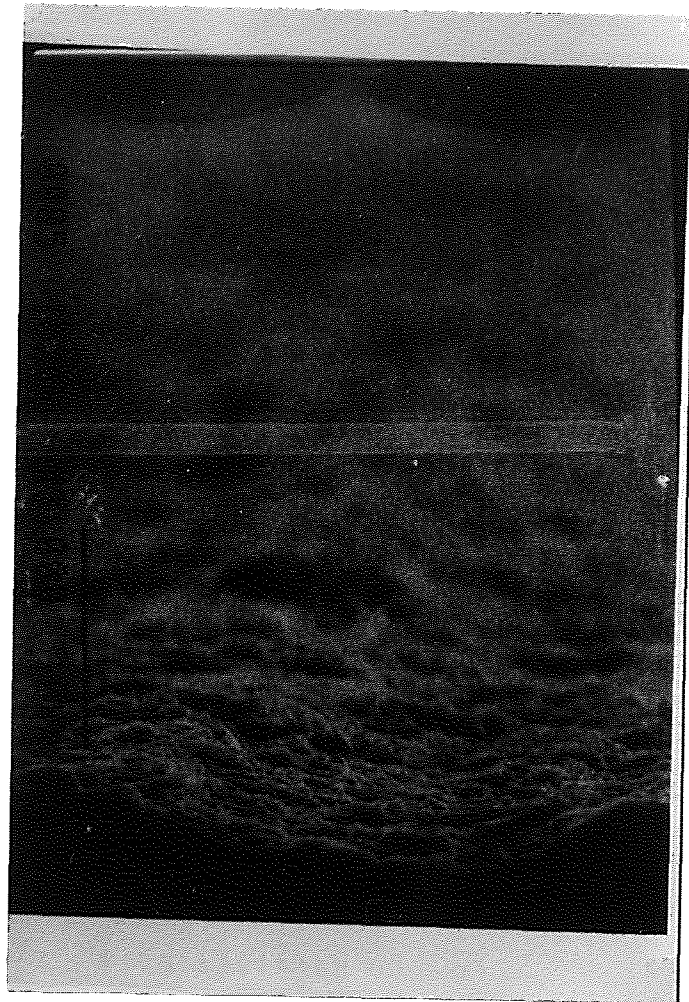

**Figure 4.19** Scanning electron micrograph of the etched pattern induced on a p-type Si (100) surface in a thin-film cell configuration in a KOH : $H_2O$ : : 1 : 20 solution. [ 30 pulses of the excimer laser were used to induce this pattern].

**Figure 4.20** Scanning electron micrograph of the etched pattern induced on a p-type Si (100) surface in a thin-film cell configuration in a KOH : $H_2O$ : : 1 : 20 solution in presence of background illumination of 1.25 mW. [ 30 pulses of the excimer laser were used to induce this pattern].

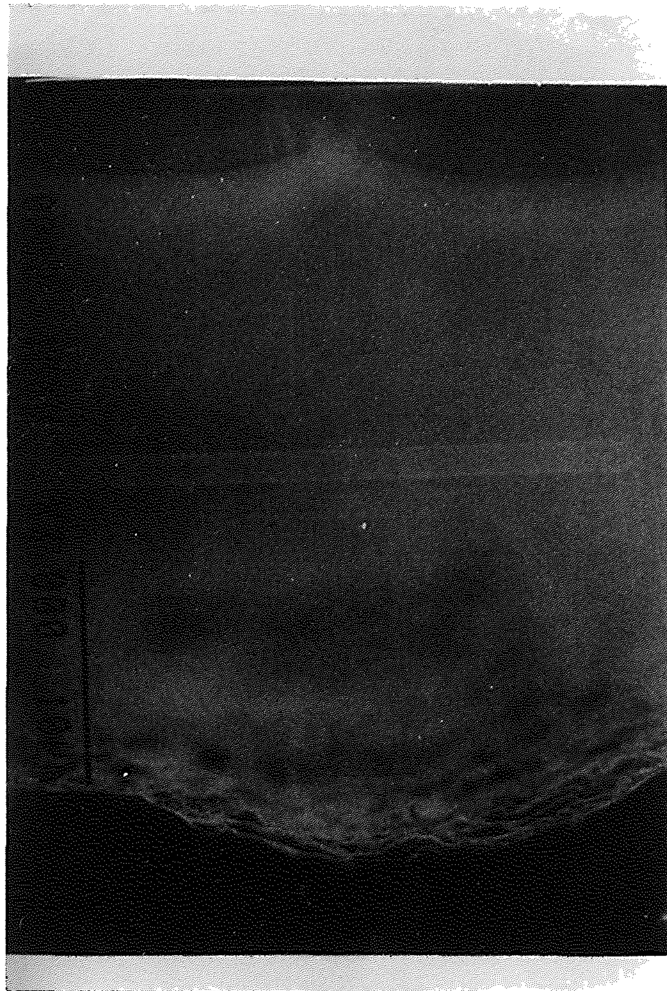

**Figure 4.21** Scanning electron micrograph of the etched pattern induced on a p-type Si (100) surface in a thin-film cell configuration in a KOH : $H_2O$ : : 1 : 20 solution in presence of background illumination of 2.50 mW. [ 30 pulses of the excimer laser were used to induce this pattern].

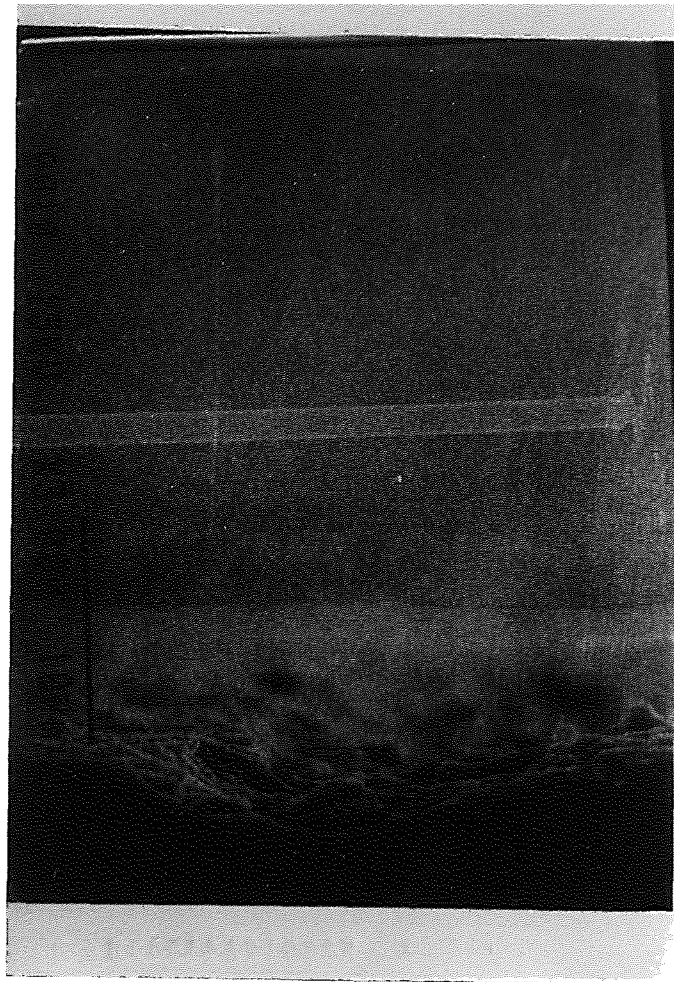

**Figure 4.22** Scanning electron micrograph of the etched pattern induced on a p-type Si (100) surface in a thin-film cell configuration in a KOH : $H_2O$ : : 1 : 20 solution in presence of background illumination of 3.75 mW. [ 30 pulses of the excimer laser were used to induce this pattern].

**Figure 4.23** Scanning electron micrograph of the etched pattern induced on a p-type Si (100) surface in a thin-film cell configuration in a KOH : $H_2O$ : : 1 : 20 solution in presence of background illumination of 5.00 mW. [ 30 pulses of the excimer laser were used to induce this pattern].

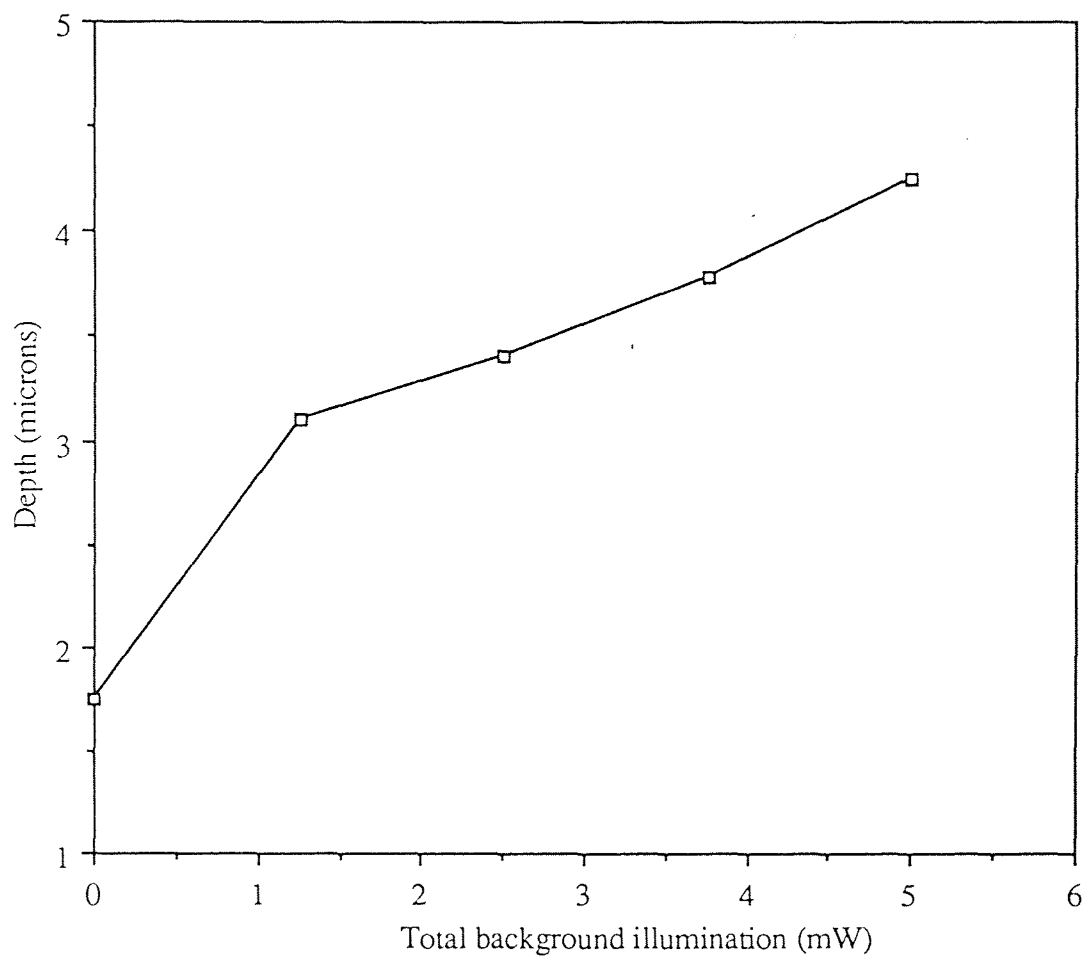


**Figure 4.24** The grating depth profile versus total background illumination for the p-type Si (100)/ KOH : $H_2O$ system. [ The points were evaluated by the SEM measurements ; 30 pulses of the excimer laser were used to induce the pattern].

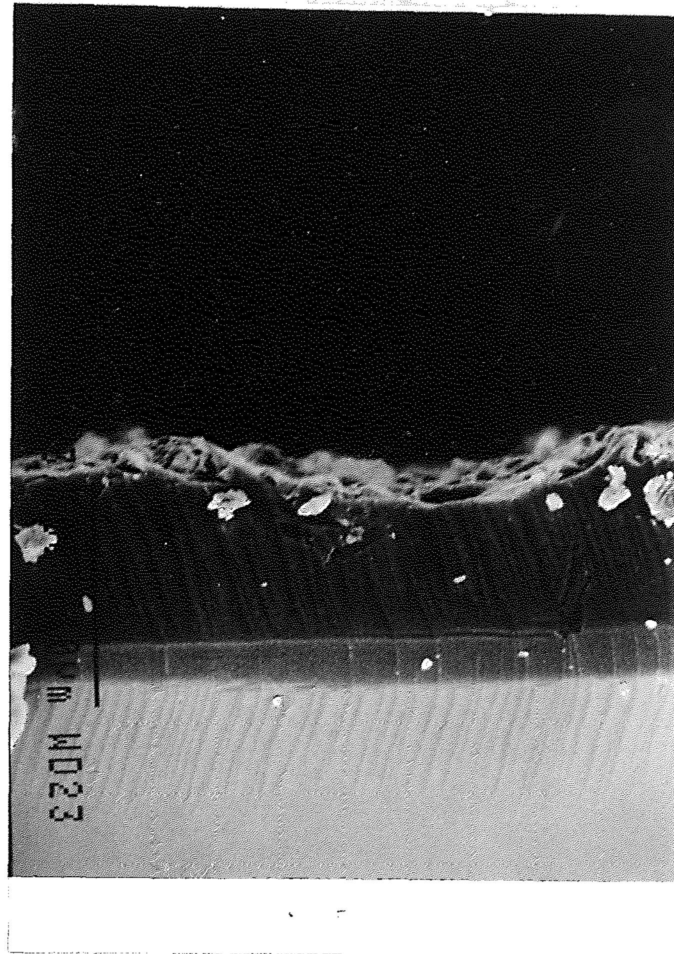


**Figure 4.25** Scanning electron micrograph of the etched pattern induced on a n-type Si (100) surface in a thin-film cell configuration in a KOH : $H_2O$ : : 1 : 20 solution. [ 30 pulses of the excimer laser were used to induce this pattern].

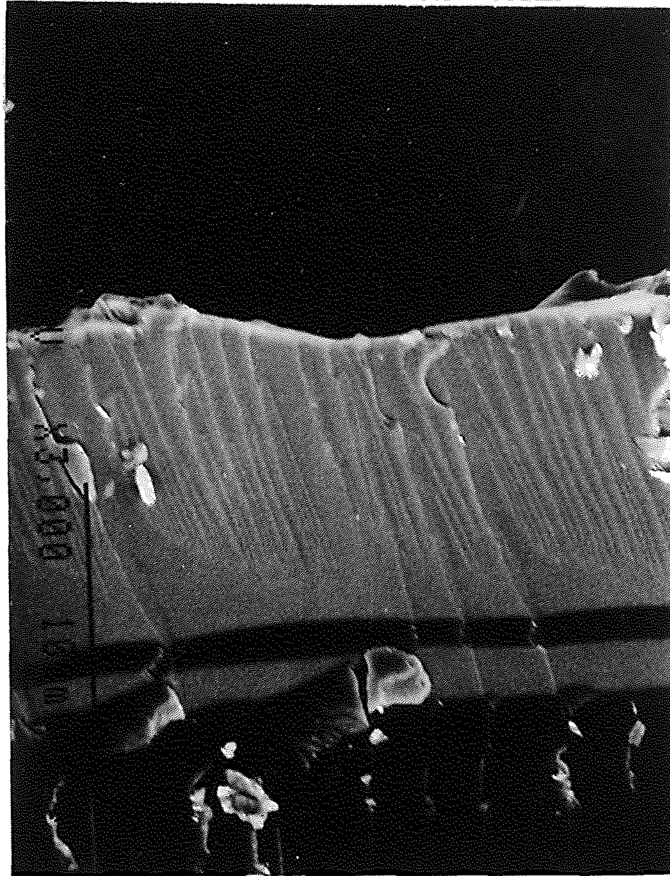

**Figure 4.26** Scanning electron micrograph of the etched pattern induced on a n-type Si (100) surface in a thin-film cell configuration in a KOH : $H_2O$ : : 1 : 20 solution in presence of background illumination of 1.25 mW. [ 30 pulses of the excimer laser were used to induce this pattern].

**Figure 4.27** Scanning electron micrograph of the etched pattern induced on a n-type Si (100) surface in a thin-film cell configuration in a KOH : $H_2O$ : : 1 : 20 solution in presence of background illumination of 2.50 mW. [ 30 pulses of the excimer laser were used to induce this pattern].

**Figure 4.28** Scanning electron micrograph of the etched pattern induced on a n-type Si (100) surface in a thin-film cell configuration in a KOH : $H_2O$ : : 1 : 20 solution in presence of background illumination of 3.75 mW. [ 30 pulses of the excimer laser were used to induce this pattern].

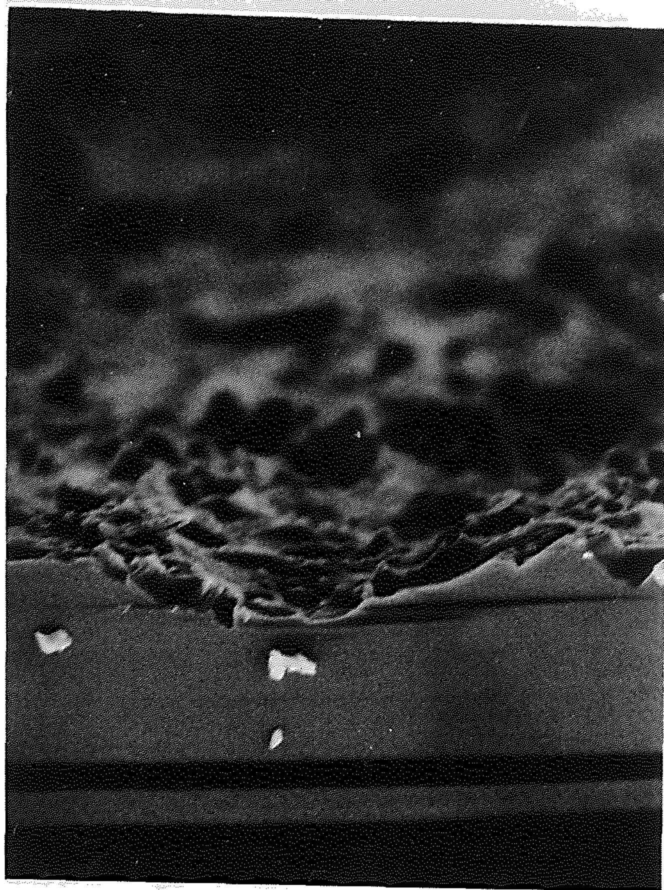

**Figure 4.29** Scanning electron micrograph of the etched pattern induced on a n-type Si (100) surface in a thin-film cell configuration in a KOH : $H_2O$ : : 1 : 20 solution in presence of background illumination of 5.00 mW. [ 30 pulses of the excimer laser were used to induce this pattern].

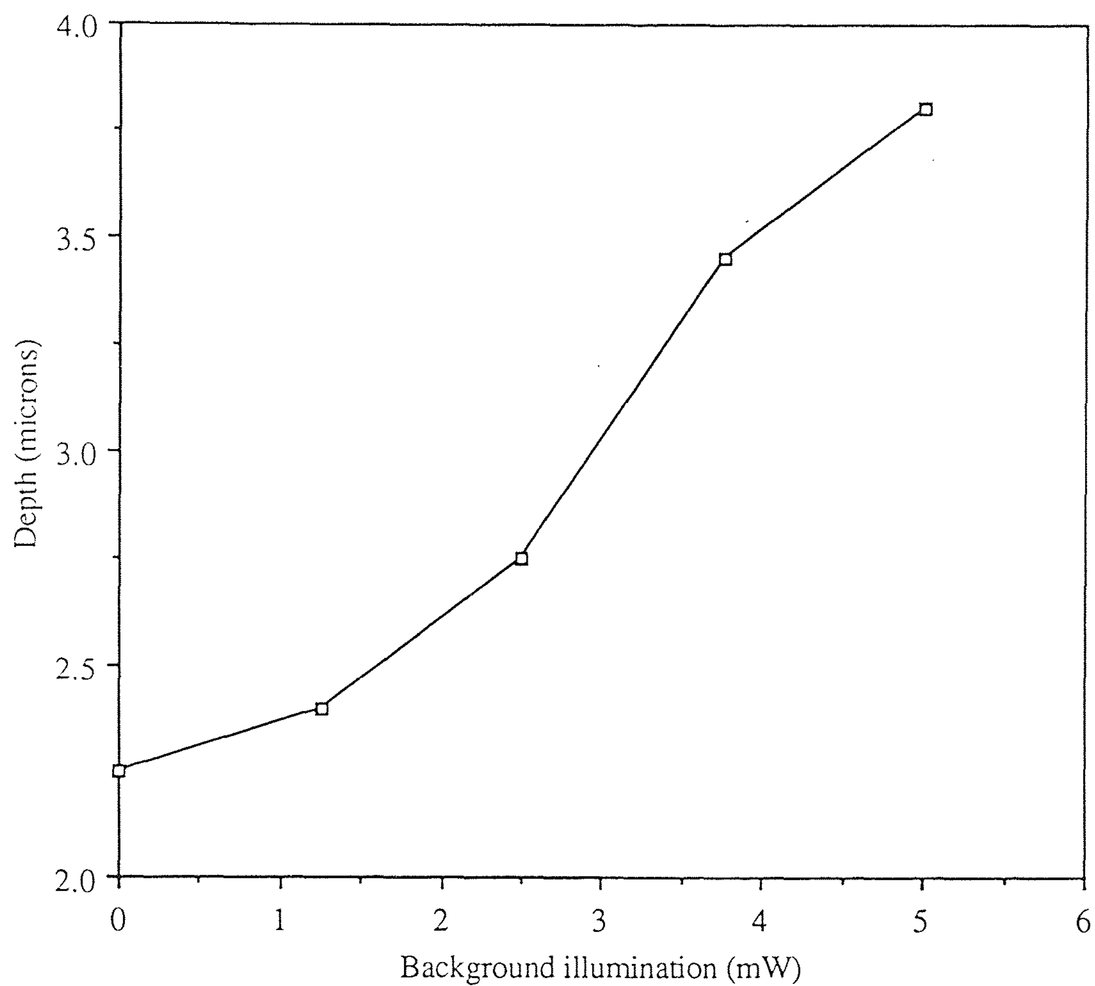


**Figure 4.30** The grating depth profile versus total background illumination for the n-type Si (100)/ KOH : $H_2O$ system. [ The points were evaluated by the SEM measurements ; 30 pulses of the excimer laser were used to induce the pattern].

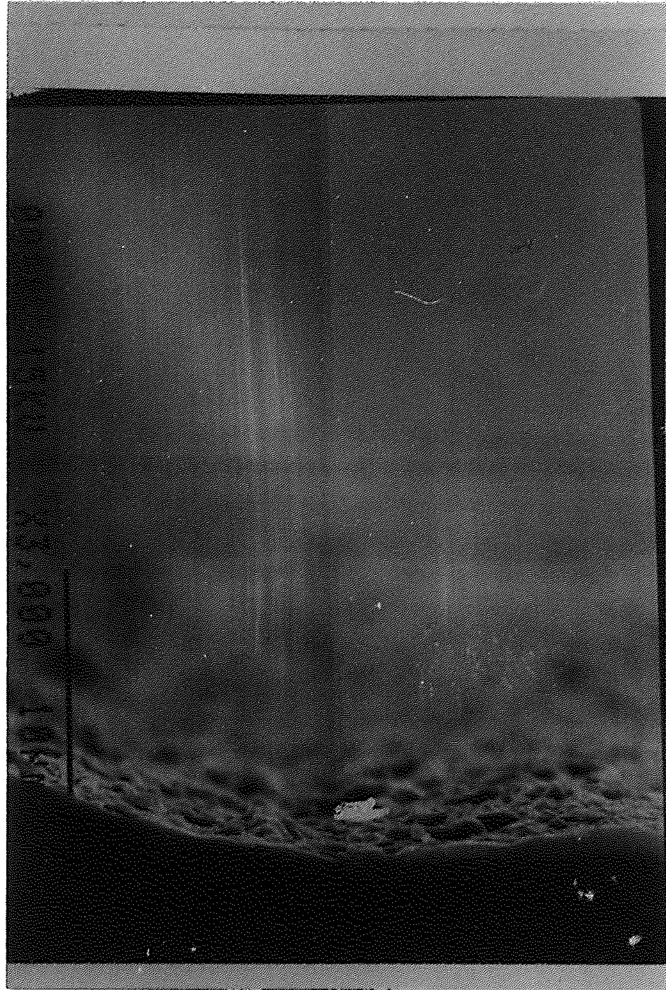

**Figure 4.31** Scanning electron micrograph of the etched pattern induced on a p-type Si (100) surface in a thin-film cell configuration in a HF : $HNO_3$ : $H_2O$ : : 2 : 3 : 100 solution without any background illumination. [ 30 pulses of the excimer laser were used to induce this pattern].

**Figure 4.32** Scanning electron micrograph of the etched pattern induced on a p-type Si (100) surface in a thin-film cell configuration in a HF : $HNO_3$ : $H_2O$ : : 2 : 3 : 100 solution with background illumination of 1.25 mW. [ 30 pulses of the excimer laser were used to induce this pattern].

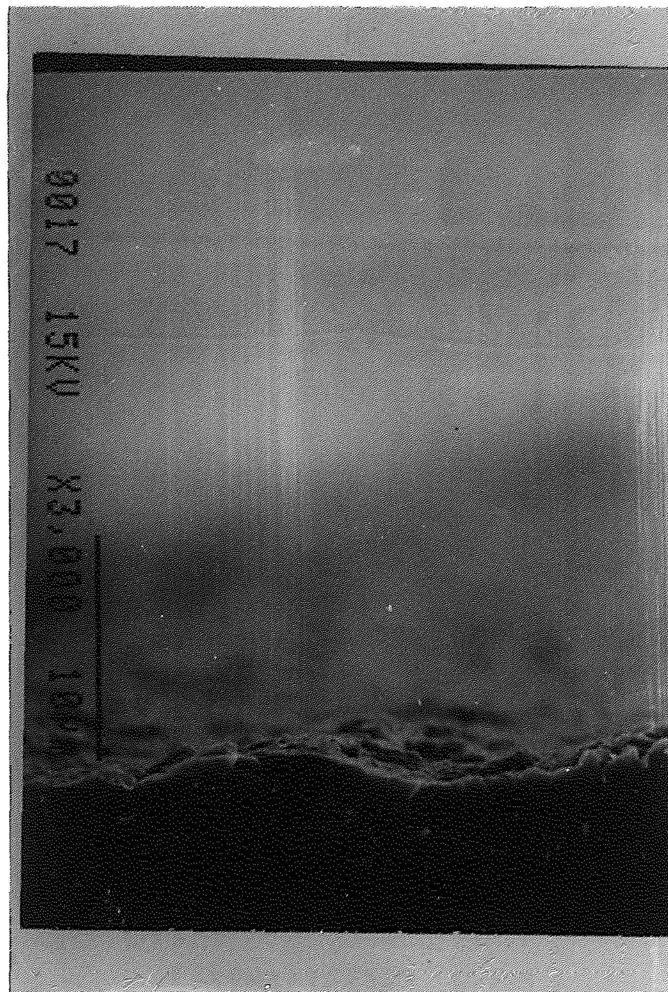


**Figure 4.33** Scanning electron micrograph of the etched pattern induced on a p-type Si (100) surface in a thin-film cell configuration in a HF : $HNO_3$ : $H_2O$ : : 2 : 3 : 100 solution with background illumination of 2.50 mW. [ 30 pulses of the excimer laser were used to induce this pattern].

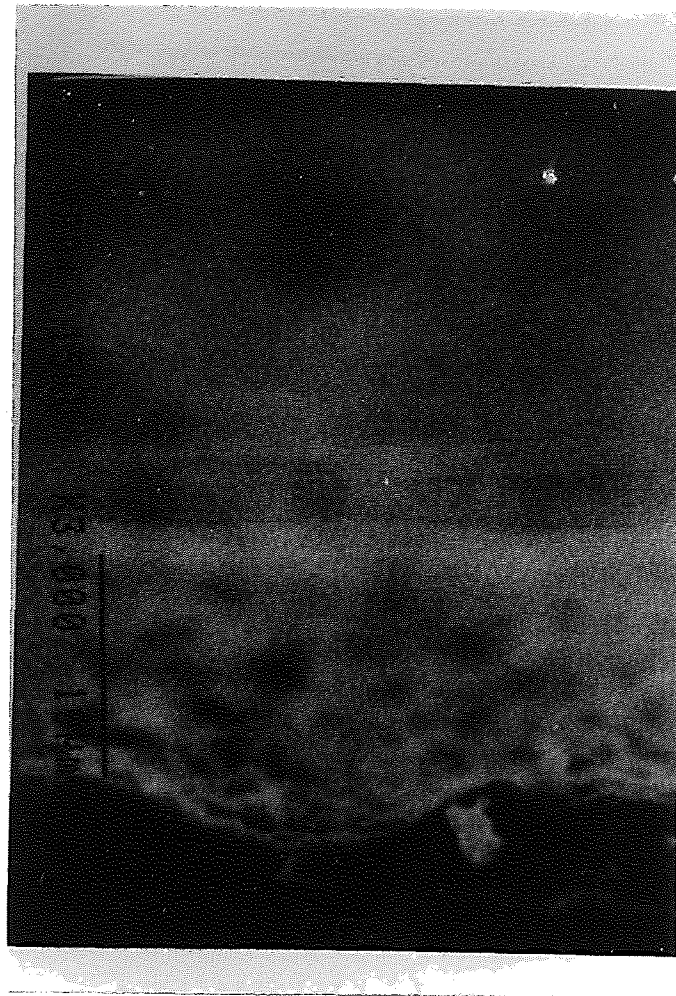


**Figure 4.34** Scanning electron micrograph of the etched pattern induced on a p-type Si (100) surface in a thin-film cell configuration in a HF : $HNO_3$ : $H_2O$ : : 2 : 3 : 100 solution with a background illumination of 3.75 mW. [ 30 pulses of the excimer laser were used to induce this pattern].

**Figure 4.35** Scanning electron micrograph of the etched pattern induced on a p-type Si (100) surface in a thin-film cell configuration in a HF : $HNO_3$ : $H_2O$ : : 2 : 3 : 100 solution with background illumination of 5.00 mW. [ 30 pulses of the excimer laser were used to induce this pattern].

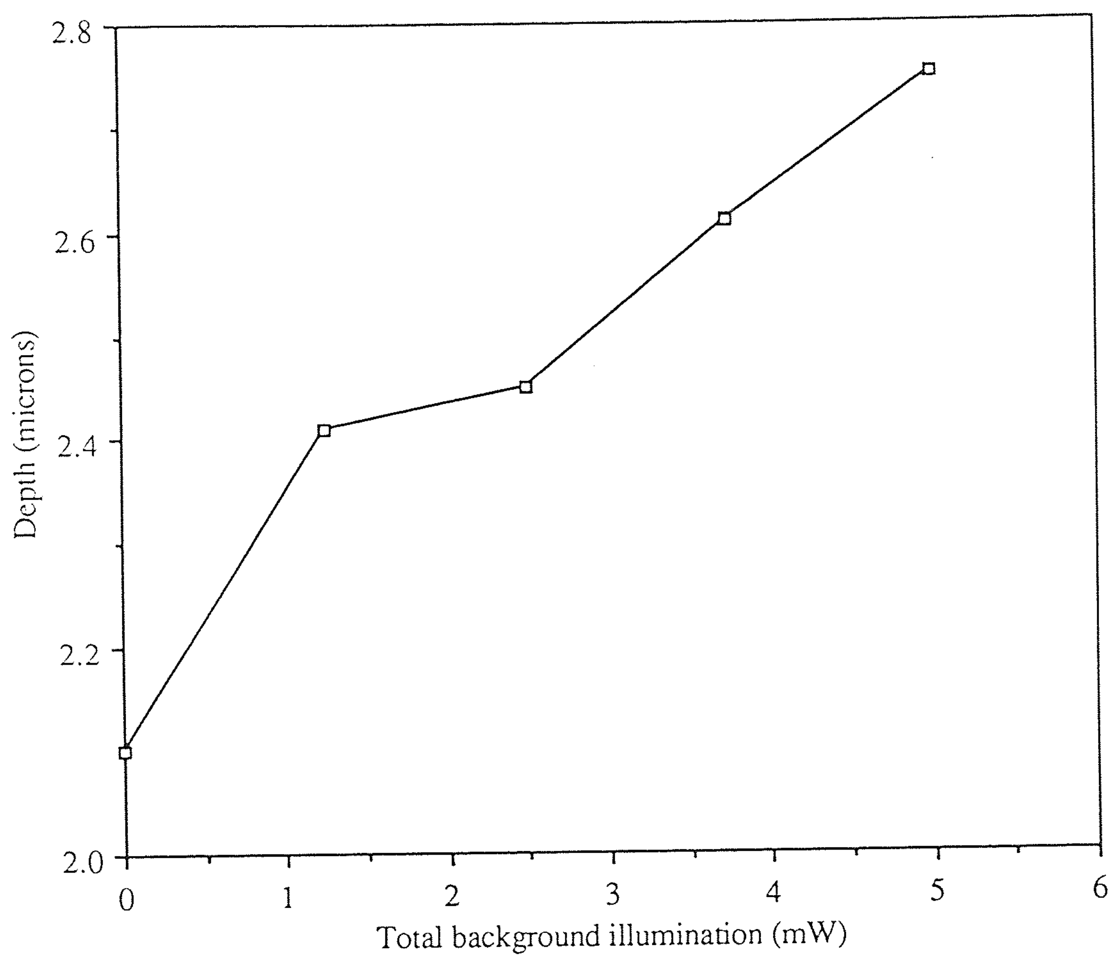


**Figure 4.36** The grating depth profile versus the total background illumination for the p-type Si(100)/HF : $HNO_3$ : $H_2O$ system. [ The points were evaluated by the SEM measurements ; 30 pulses of the excimer laser were used to induce the pattern].

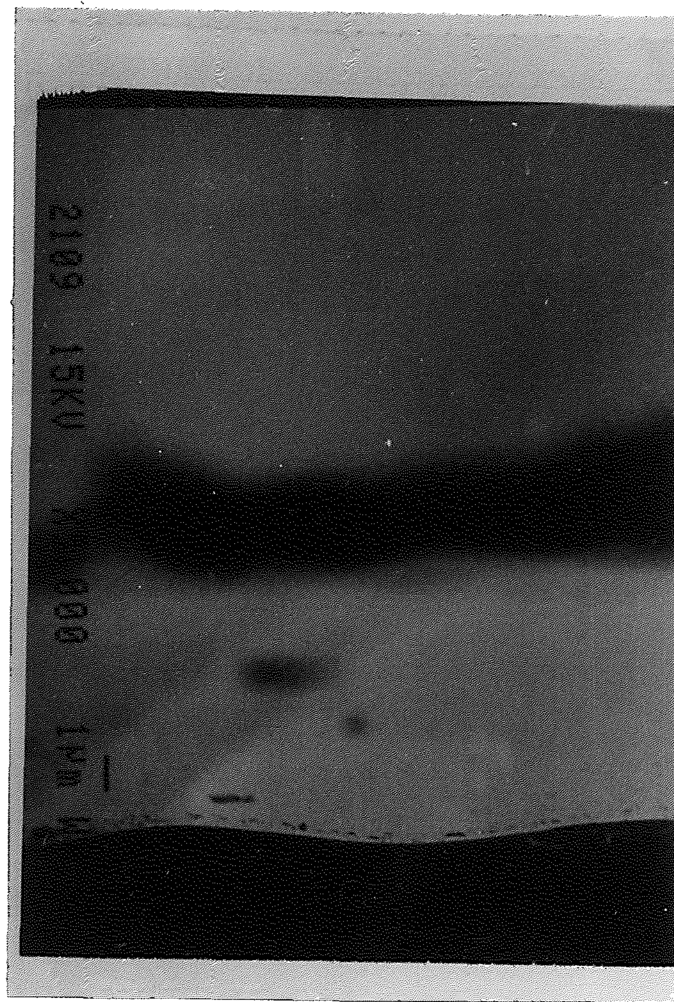


**Figure 4.37** Scanning electron micrograph of the etched pattern induced on a n-type Si (100) surface in a thin-film cell configuration in a KOH : $H_2O$ : : 1 : 20 solution without any background illumination. [ 20 pulses of the excimer laser were used to induce this pattern].

**Figure 4.38** Scanning electron micrograph of the etched pattern induced on a n-type Si (100) surface in a thin-film cell configuration in a KOH : $H_2O$ : : 1 : 20 solution with a background illumination of 1.25 mW. [ 20 pulses of the excimer laser were used to induce this pattern].

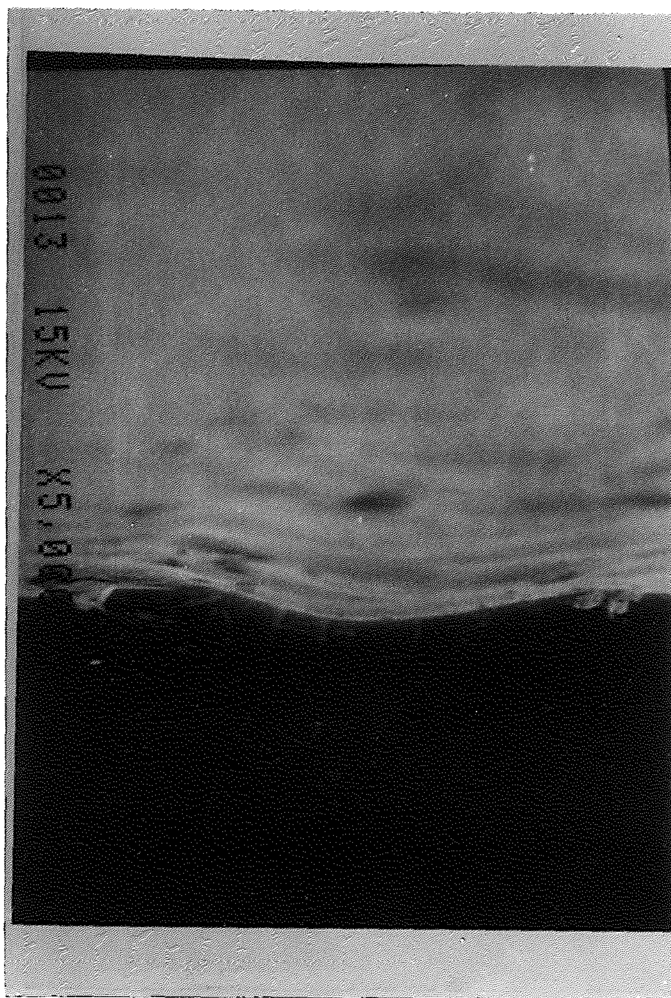


**Figure 4.39** Scanning electron micrograph of the etched pattern induced on a n-type Si (100) surface in a thin-film cell configuration in a KOH : $H_2O$ : : 1 : 20 solution with a background illumination of 3.75 mW. [ 20 pulses of the excimer laser were used to induce this pattern].

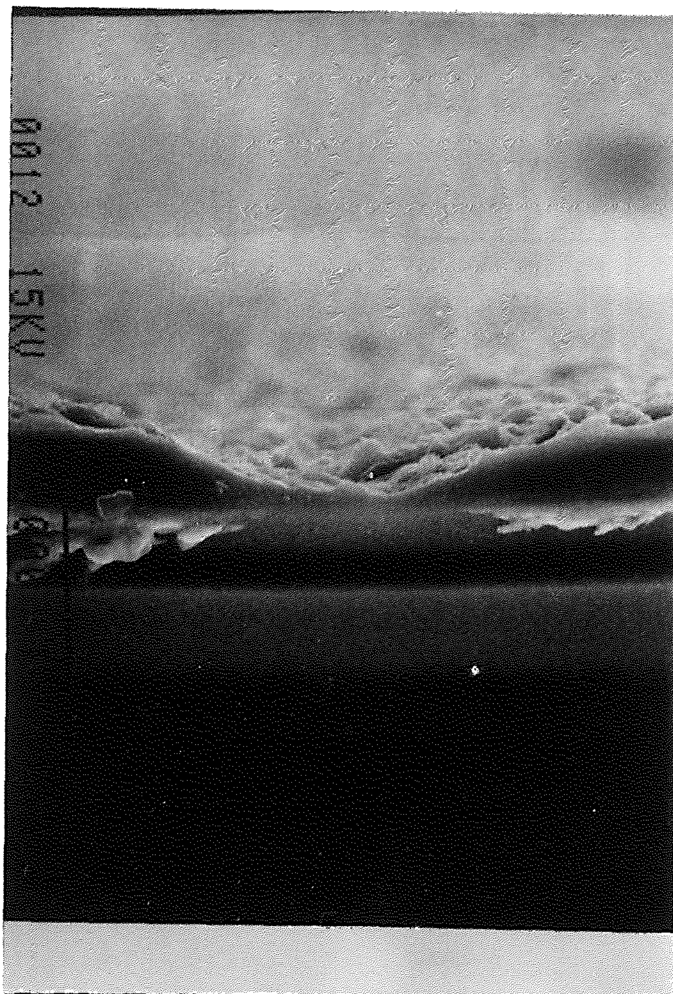


**Fig. 4.40** Scanning electron micrograph of the etched pattern induced on a n-type Si (100) surface in a thin-film cell configuration in a KOH : $H_2O$ : : 1 : 20 solution with a background illumination of 5.00 mW. [ 20 pulses of the excimer laser were used to induce this pattern].

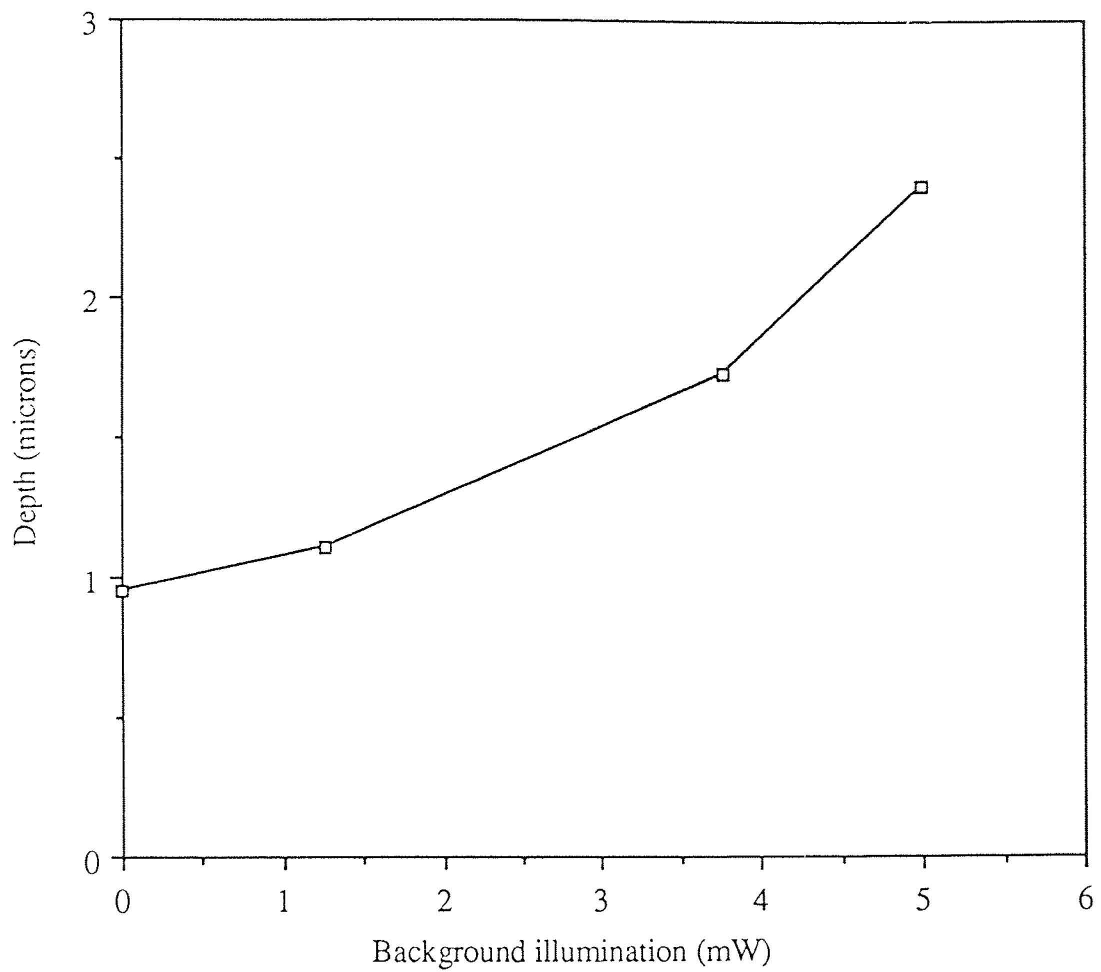


**Figure 4.41** The grating depth profile versus the total background illumination for the n-type Si (100)/ KOH : $H_2O$ system. [ The points were evaluated by the SEM measurements ; 20 pulses of the excimer laser were used to induce the pattern].

**Table 4.1** Light Diffraction Intensity Measurement Data from Grooves of Samples 1 and 2. ( The incident angle $\phi i$ of the probe beam HeNe ( $\lambda$ = 633 nm ) is 17. 31° and the measurement distance [ d ] is 265 mm ).

| SAMPLE | | 1 | 2 |
|---|---|---|---|
| PERIOD | | 15 μm | 15 μm |
| $I_{00}$ | | 0. 4750 | 0. 4750 |
| | X ( mm ) | Intensity | Intensity |
| $I_{+3}$ | 5.00 | 0.0024 | 0.0040 |
| $I_{+2}$ | 6.50 | 0.0050 | 0.0072 |
| $I_{+1}$ | 8.00 | 0.0119 | 0.0124 |
| $I_{0}$ | 9.00 | 0.4250 | 0.4260 |
| $I_{-1}$ | 10.50 | 0.0112 | 0.0112 |
| $I_{-2}$ | 11.50 | 0.0062 | 0.0065 |
| $I_{-3}$ | 13.00 | 0.0045 | 0.0020 |

**Table 4.2** Light Diffraction Intensity Measurement Data from Grooves of Samples 3 and 4. ( The incident angle $\phi i$ of the probe beam HeNe ( $\lambda$ = 633 nm ) is 17. 31° and the measurement distance [ d ] is 265 mm ).

| SAMPLE | | 1 | 2 |
|---|---|---|---|
| PERIOD | | 15 μm | 15 μm |
| $I_{00}$ | | 0. 4750 | 0. 4750 |
| | X ( mm ) | Intensity | Intensity |
| $I_{+3}$ | 5.00 | 0.0045 | 0.0060 |
| $I_{+2}$ | 6.50 | 0.0091 | 0.0083 |
| $I_{+1}$ | 8.00 | 0.0192 | 0.0154 |
| $I_{0}$ | 9.00 | 0.4161 | 0.4249 |
| $I_{-1}$ | 10.50 | 0.0302 | 0.0186 |
| $I_{-2}$ | 12.00 | 0.0111 | 0.0068 |
| $I_{-3}$ | 13.50 | 0.0056 | 0.0032 |

**Table 4.3** Light Diffraction Intensity Measurement Data from Grooves of Samples 5 and 6. (The incident angle $\phi$i of the probe beam HeNe ( $\lambda$ = 633 nm ) is 17. 31° and the measurement distance [ d ] is 265 mm ).

| SAMPLE | | 1 | 2 |
|---|---|---|---|
| PERIOD | | 15 μm | 15 μm |
| $I_{00}$ | | 0. 4780 | 0. 4770 |
| | X ( mm ) | Intensity | Intensity |
| $I_{+3}$ | 4.50 | 0.0072 | 0.0045 |
| $I_{+2}$ | 6.00 | 0.0091 | 0.0095 |
| $I_{+1}$ | 7.50 | 0.0192 | 0.0140 |
| $I_{0}$ | 8.50 | 0.4161 | 0.4175 |
| $I_{-1}$ | 9.50 | 0.0302 | 0.0210 |
| $I_{-2}$ | 11.00 | 0.0111 | 0.0080 |
| $I_{-3}$ | 13.00 | 0.0056 | 0.0039 |

**Tab 4.4** Light Diffraction Intensity Measurement Data from Grooves of Samples 7 and 8. (The incident angle φi of the probe beam HeNe ( λ = 633 nm ) is 17. 31° and the measurement distance [ d ] is 265 mm ).

| SAMPLE | | 1 | 2 |
|---|---|---|---|
| PERIOD | | 15 μm | 15 μm |
| $I_{00}$ | | 0. 4780 | 0. 4770 |
| | X ( mm ) | Intensity | Intensity |
| $I_{+3}$ | 5.00 | 0.0064 | 0.0082 |
| $I_{+2}$ | 6.50 | 0.0095 | 0.0115 |
| $I_{+1}$ | 8.00 | 0.0285 | 0.0275 |
| $I_0$ | 9.00 | 0.3960 | 0.3850 |
| $I_{-1}$ | 10.00 | 0.0239 | 0.0265 |
| $I_{-2}$ | 11.50 | 0.0150 | 0.0085 |
| $I_{-3}$ | 13.00 | 0.0040 | 0.0069 |

**Tab 4.5** Light Diffraction Intensity Measurement Data from Grooves of Samples 9 and 10. (The incident angle $\phi i$ of the probe beam HeNe ( $\lambda$ = 633 nm ) is 17. 31° and the measurement distance [ d ] is 265 mm ).

| SAMPLE | | 1 | 2 |
|---|---|---|---|
| PERIOD | | 15 μm | 15 μm |
| $I_{00}$ | | 0. 4750 | 0. 4750 |
| | X ( mm ) | Intensity | Intensity |
| $I_{+3}$ | 5.50 | | 0.0105 |
| $I_{+2}$ | 7.00 | 0.0212 | 0.0150 |
| $I_{+1}$ | 8.50 | 0.0315 | 0.0301 |
| $I_0$ | 9.50 | 0.3846 | 0.3620 |
| $I_{-1}$ | 10.50 | 0.0310 | 0.0286 |
| $I_{-2}$ | 12.00 | 0.0071 | 0.0115 |
| $I_{-3}$ | 13.50 | 0.0038 | 0.0090 |

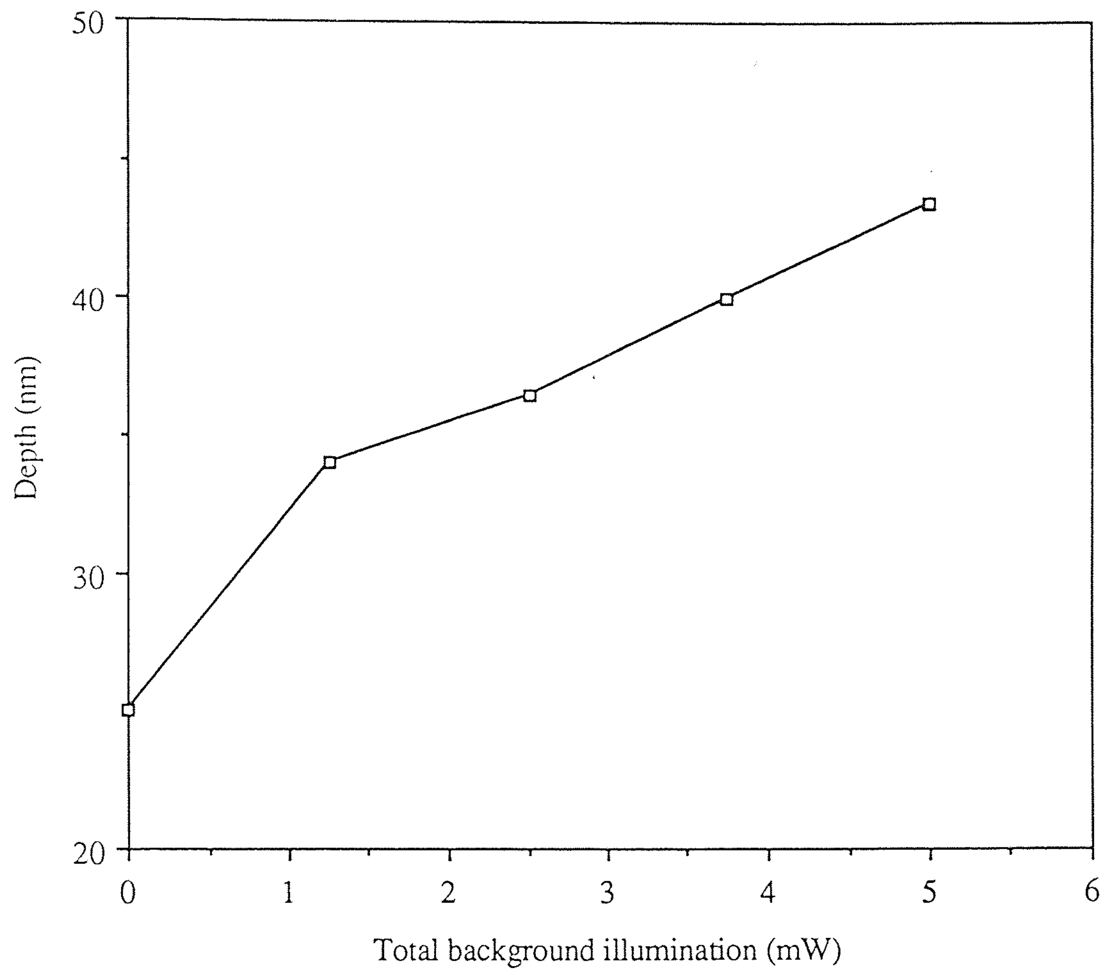


**Figure 4. 42** The grating depth profile versus total background illumination for the p-type Si (100)/ KOH : $H_2O$ system. [ The points were evaluated by the light diffraction measurement technique ; only 1 pulse of the excimer laser was used to induce the pattern].

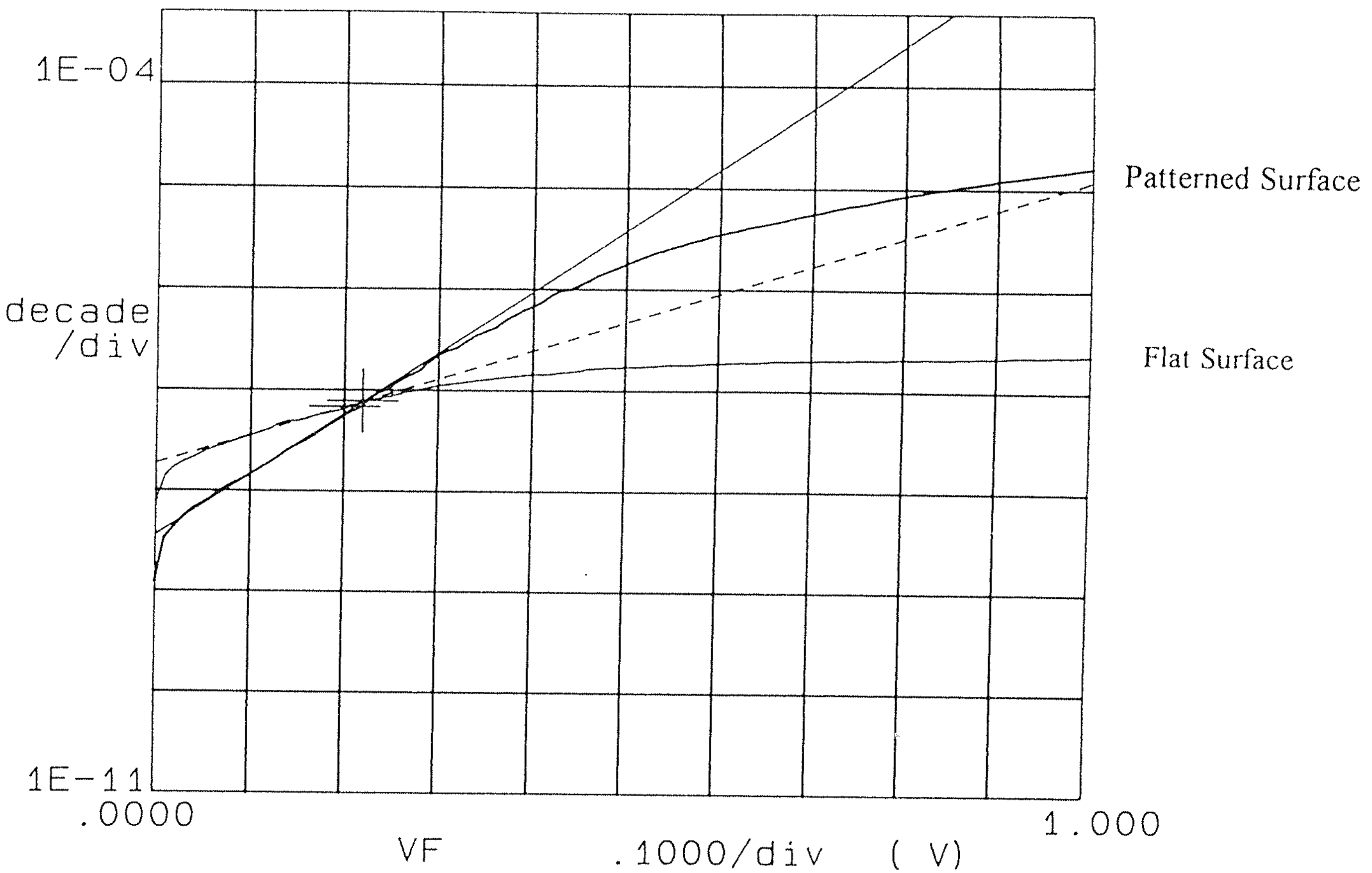


**Figure 4.43** Forward current-voltage ( I-V ) characteristics of Al / p-type Si (100) contacts both on the patterned and flat surfaces of the sample number 1.

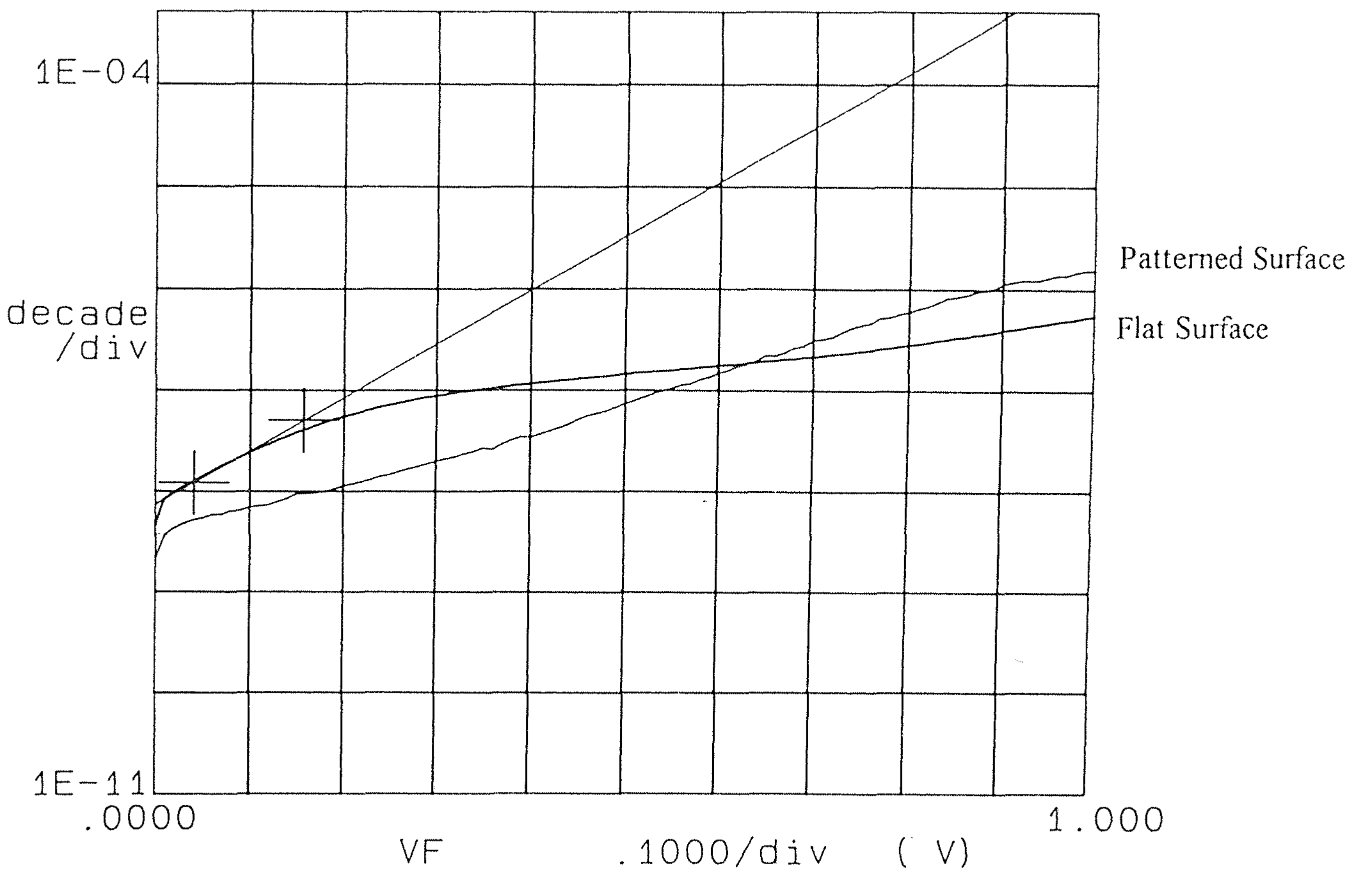


**Figure 4.44** Forward current-voltage ( I-V ) characteristics of Al / p-type Si (100) contacts both on the patterned and flat surfaces of the sample number 2.

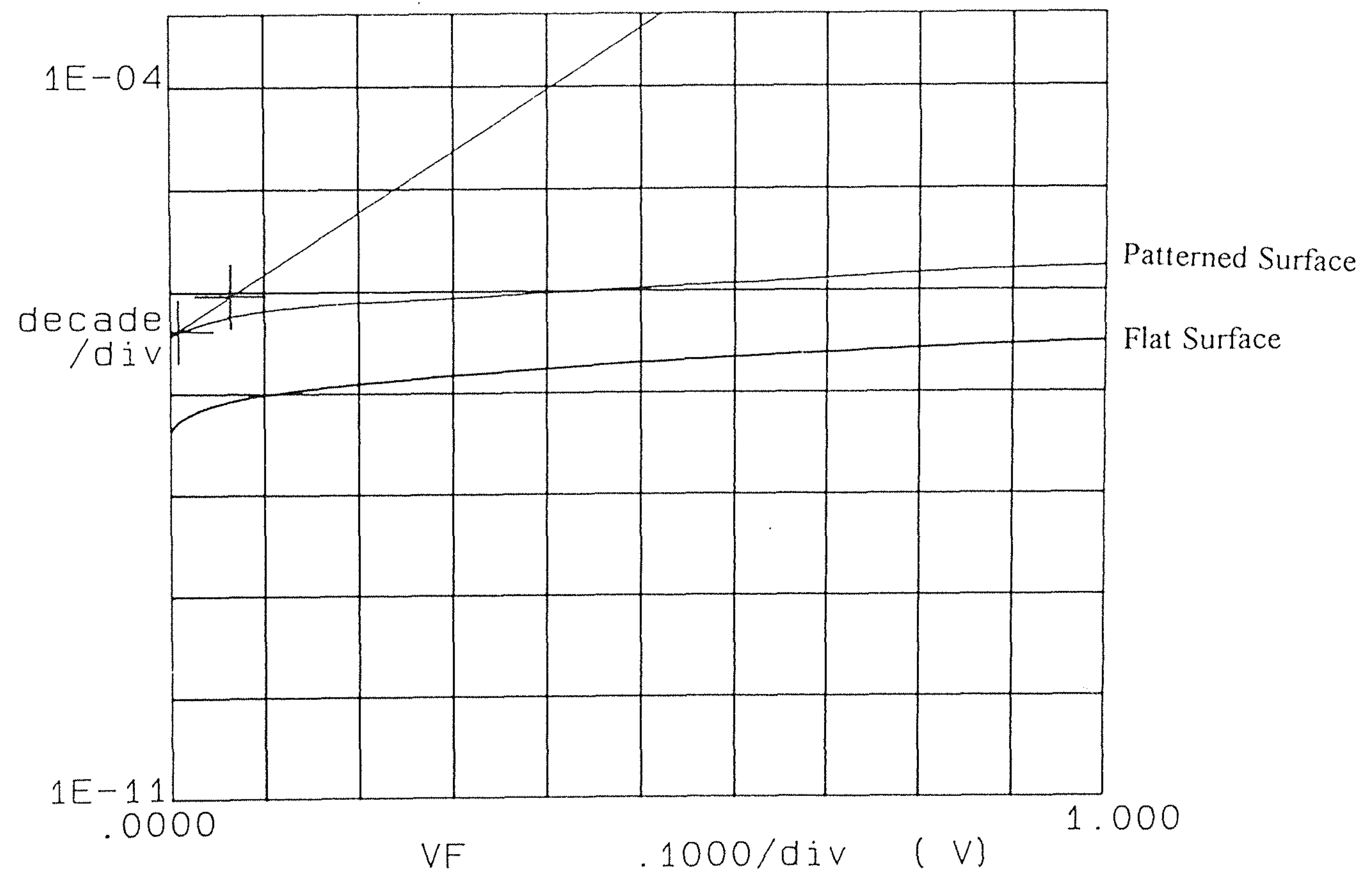


**Figure 4.45** Forward current-voltage ( I-V ) characteristics of Al / p-type Si (100) contacts both on the patterned and flat surfaces of the sample number 3.

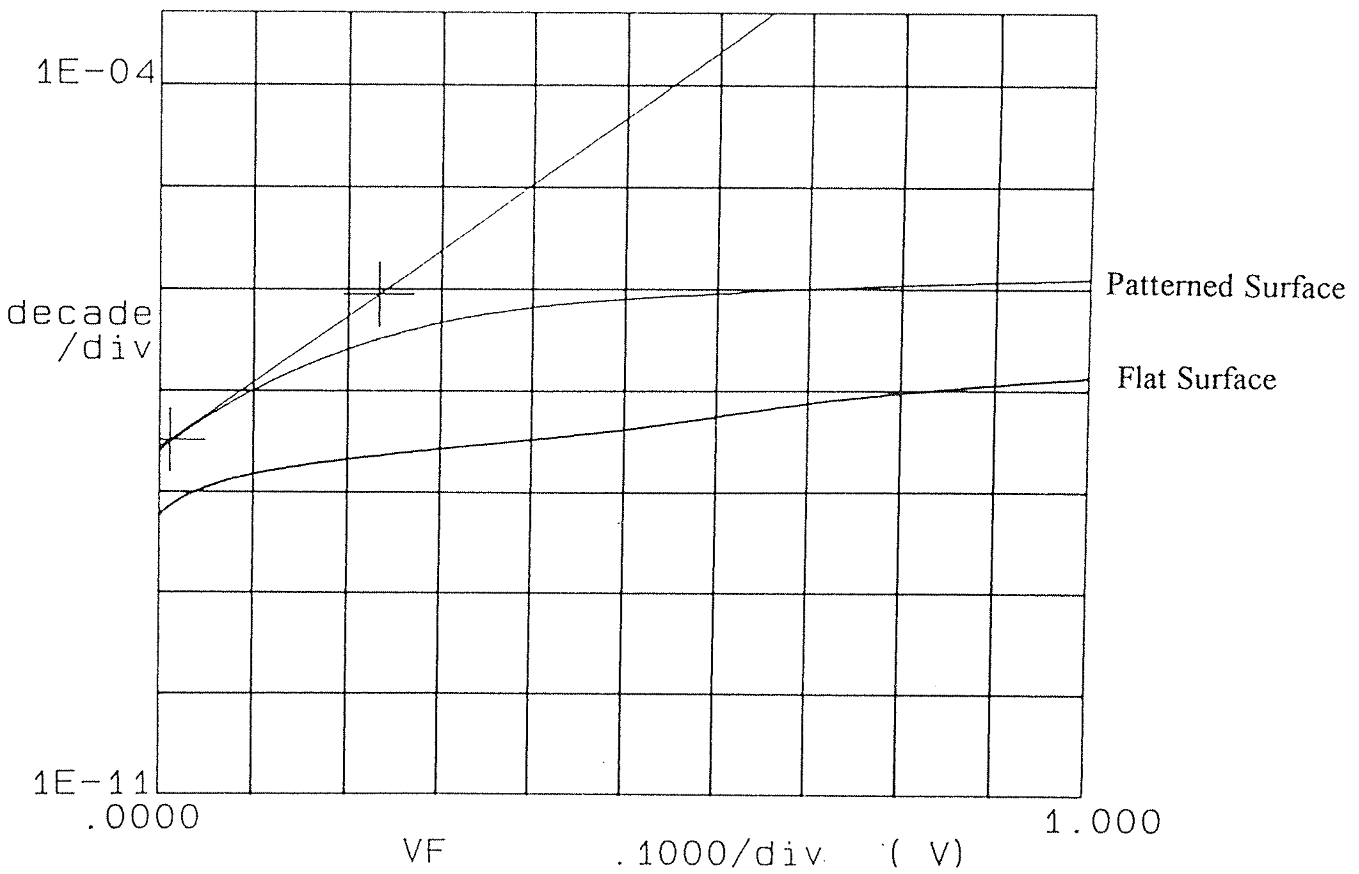


**Figure 4.46** Forward current-voltage ( I-V ) characteristics of Al / p-type Si (100) contacts both on the patterned and flat surfaces of the sample number 4.

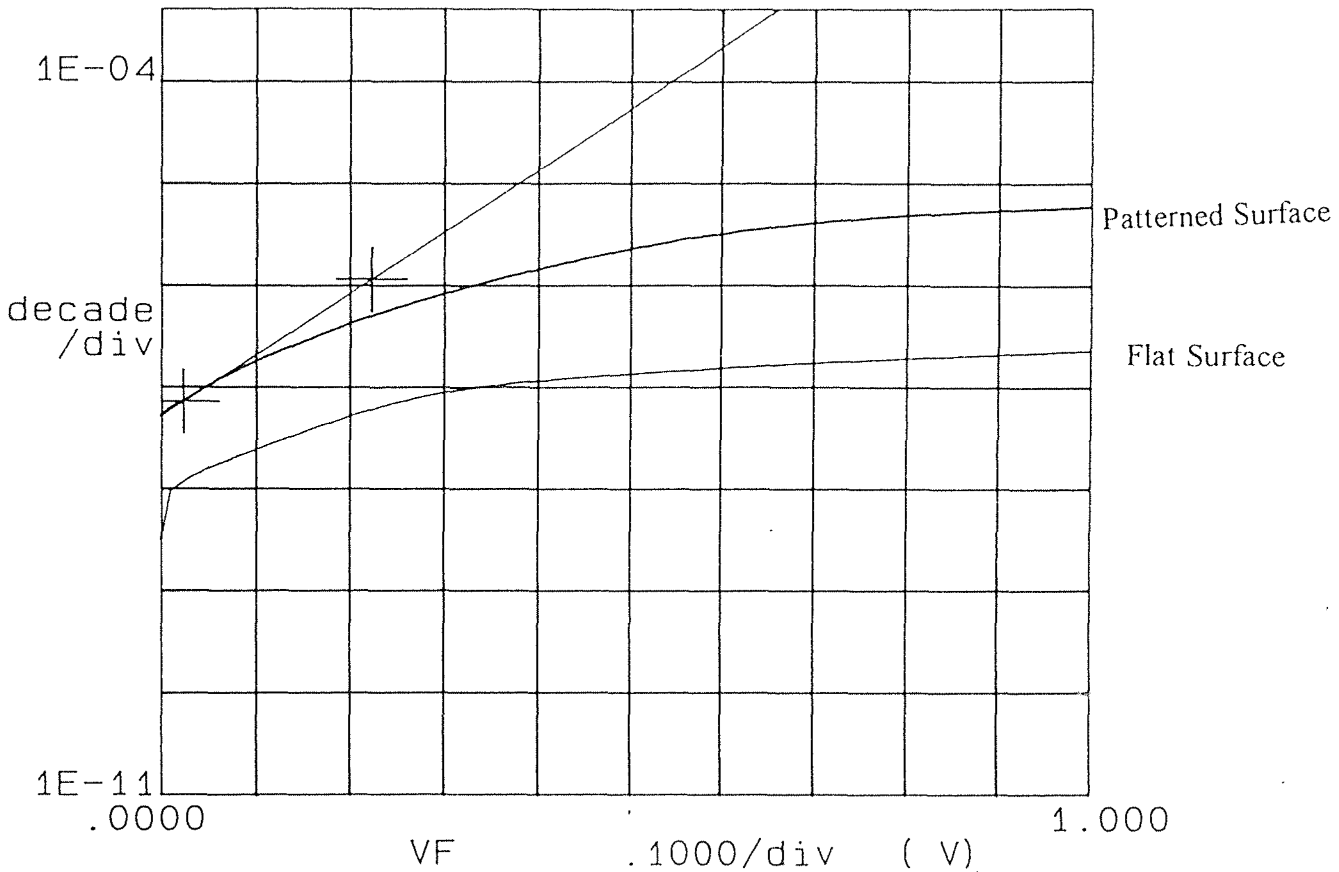


**Figure 4.47** Forward current-voltage ( I-V ) characteristics of Al / p-type Si (100) contacts both on the patterned and flat surfaces of the sample number 5.

**Table 4.6** Metal-Semiconductor Barrier Height Determination.

| Sample Number | Contact Areas ($cm^2$)<br>a. flat area<br>b.patterned area | period (µm) | Depth (nm) | Sasuration Current ($A/cm^2$)<br>a. flat area<br>b. patterned area | Barrier Height (V)<br>a. flat area<br>b.pattern-area |
|---|---|---|---|---|---|
| 1 | a. $3.14 \times 10^{-2}$<br>b. $4.44 \times 10^{-2}$ | 15 | 15 | a. $18.70 \times 10^{-9}$<br>b. $3.60 \times 10^{-9}$ | a. 0.79<br>b. 0.84 |
| 2. | a. $3.14 \times 10^{-2}$<br>b. $4.44 \times 10^{-2}$ | 15 | 25 | a. $7.25 \times 10^{-9}$<br>b. $5.50 \times 10^{-9}$ | a. 0.81<br>b. 0.83 |
| 3 | a. $0.785 \times 10^{-2}$<br>b. $0.785\times 10^{-2}$ | 125 | 5000 | a. $75.0 \times 10^{-9}$<br>b. $368 \times 10^{-9}$. | a. 0.71<br>b. 0.68 |
| 4 | a. $0.785 \times 10^{-2}$<br>b. $0.785 \times 10^{-2}$ | 250 | 5000 | a. $8.25 \times 10^{-9}$<br>b. $2.71 \times 10^{-9}$ | a. 0.77<br>b. 0.74 |
| 5 | a. $3.14 \times 10^{-2}$<br>b. $3.14 \times 10^{-2}$ | 375 | 5000 | a. $9.26 \times 10^{-9}$<br>b. $51.40 \times 10^{-9}$ | a. 0.80<br>b. 0.76 |

# CHAPTER 5

# DISCUSSION

In this thesis, we have demonstrated that the depth of an ablated profile of silicon induced by an excimer laser ( $\lambda$ =248 nm, and power $\approx$ 0.25 watt with a repetition rate of 10 Hz ) in air varies linearly with the number of pulses of the irradiated beam. This data can be interpreted as silicon ablation rate ( μm/ pulse) Vs the energy density ( $J/cm^2$). We note that the periodic surface corrugation can be produced without having any mask or using any holographic technique.

We have also demonstrated the effect of a secondary light source, He-Ne laser, ( $\lambda$ = 633 nm, and power $\approx$ 5 mW of a spot size of 1 mm diameter ) on the ablation rate of the silicon effected by the excimer laser. We have reported that a secondary light source has virtually no effect on the ablation rate in air. This demonstrates that there is no coupling effect between the ultraviolet, excimer laser and the infra-red, He-Ne laser at the energy indicated.

In this thesis, we have demonstrated that a wet-chemical etching technique ( for both the Si (100)/ KOH : $H_2O$ and Si (100)/ HF: $HNO_3$ : $H_2O$ systems) is a more effective method of mass removal rate than the air ablation method. In this thesis, we have emphasized the importance of the use of an additional light source to affect the etching rate. We have established the fact that the secondary light source, He-Ne laser ( $\lambda$ = 633 nm and power $\approx$ 5 mW of a spot size of 1 mm diameter) increases the etching rate induced by the etching beam. We have established that fact for both the Si (100)/ KOH : $H_2O$ and Si (100)/ HF : $HNO_3$ : $H_2O$ systems. We have obtained the same trend of the results both for the n-type and p-type silicon. Silicon sample in an 'as is' condition as well as treated surface condition demonstrates the same trend. All the analyses of the patternings mentioned here have been done by the

scanning electron microscope (SEM). Finally, we have verified the fact that the background light increases the etching rate by light diffraction technique for n-type Si(100)/ KOH :$H_2O$ system.

Our experimental findings contradicts the findings of Willner et al. [22]. They have established their results for the n-InP/ HF : $H_2O$ and a CW laser system. According to their results, a secondary light source reduces the surface potential, which in turn decreases the etching efficiency induced by the photo-generated carriers. In their model they have assumed that the voltage drop occurs only across the semiconductor surface depletion layer and no voltage drop occurs across the Helmholtz layer. Willner et al. have established the fact that etch rate decreases rapidly with low secondary light intensity ( i.e., at around 0.3 mW) and then saturates as the controller light is increased (i.e., at around 2.5 mW). We believe that background light also takes part with the etching beam in the generation of hole-electron pairs in a thin-film cell configuration. The enhanced etching rate in presence of background illumination is probably due to a better UV coupling with the silicon surface. We note that we have used the pulsed excimer laser, not the Continuous Wave doubled argon laser as used by Willner et al.

In our thesis, we have demonstrated that surface patterning has a pronounced effect on the barrier height of the metal-semiconductor contact. We have reported the patterning effect on the barrier height by varying the depth and periodicity of the groove profiles on silicon surfaces. The metal-semiconductor barrier height can be increased by producing very shallow ($\approx$ 15-25 nm ) and short pitch ( 15 μm ) surface patterning. The barrier heights of the contacts on patterned surface are higher than those made on the flat surfaces. But the interesting fact is that the barrier heights of the metal-semiconductor contacts were greatly reduced compared to those on the flat surfaces when the periodicity ( i.e., 125, 250, and 375 - μm ) and

the depth ( e.g., $\approx 5\ \mu m$ ) of the grating profiles have been increased. Barrier height decrease may be attributed to the sharp structures in the surface relief. We note that the increase in the area owing to the relief has been taken into account in the calculations.

# CHAPTER 6

# CONCLUSION

We have produced periodic surface structures using the Ultraviolet excimer laser both in air and liquid phases. We have studied a thin-film cell configuration for the laser-aided electrochemical etching and investigated the grating profiles under different conditions.

We have reported the use of a secondary light source as background illumination as an etch enhancement source. The study of the surface corrugation by the scanning electron micrographs has made it obvious to us that the secondary light source enhance the etching rate. We have unequivocally verified this fact by measuring the grating profile using the light diffraction intensity measurement technique.

We have also reported that periodic surface patterning of the semiconductor for metal-semiconductor contacts affects the potential barrier height. The corrugations on silicon wafers generally decreased the barrier height of metal-semiconductor contacts as measured by the current-voltage ( I-V ) method.

## REFERENCES


1. K.G. Ibbs and R. M. Osgood, Laser Chemical Processing for Microelectronics, Cambridge Studies in Modern Optics 7, Camdridge University Press, (1989) : 1-24, 109-145.

2. E. Fogarassy, C. Fuchs, A. Slaoui, and J. P. Stoquert, *Appl. Phys. Lett.* 57 (7), 664 (1990)

3. A. Slaoui, E. Fogarassy, C. Fuchs, and P. Siffert, *J. Appl. Phys.* 71 (2), 590 (1992).

4. M. Hanabusa and M. Suzuki, *Appl. Phys. Lett.* 39, 431 (1981).

5. C. Garban-Labaune, E. Fabre, C.E. Max, R. Fabbro, F. Amiranoff, J. Virmont, M. Weinfeld, and Michard, *Phys. Rev. Lett.* 48, 1018 ( 1982).

6. Kouichi Murakami, Hans C. Gerristen, Hedser van Brug, Fred Bijkerk, Frans W. Saris, and Marnix J. van der Wiel, *Phys. Rev. Lett.* 56, 655 (1986).

7. G. Gorodetsky, Jery Kanicki, T. Kazyaka, and R. L. Melcher, *Appl. Phys. Lett.* 46(6), 547 ( 1985).

8. H. van Brug, K. Murakami, F. Bijkerk, and M. J. van der Wiel, *J. Appl. Phys.* 60 (10), 3438 (1986).

9. J. F. Ready, Effects of High Power Laser Radiation (Academic, New York, 1984).

10. P. M. Fauchet and A. E. Siegman, *Appl. Phys. Lett.* 40 (9), 824 (1982).

11. J. F. Young, J. F. Sipe, J. S. Preston, and H. M. von Driel, *Appl. Phys. Lett.* 41, 261 (1982).

12. D. J. Ehrlich, R. M. Osgood , *IEEE Electron. Dev. Lett.* **EDL-1**, 101 (1980).

13. P. A. Kohl, C. Wolowodiuk, and F. J. Ostermayer, *J. Electrochem. Soc.* 130, 2288 (1983).

14. M. Lax, *Appl. Phys. Lett.* 33, 786 (1978).

15. J. I. Steinfeld, T.G. Anderson, C. Reisner, D. R. Denison, L. D. Hartsough, and J.R. Hollahan, *J Electrochem. Soc.* 127, 514 (1980).

16. D. L. Kendall, *Appl. Phys. Lett.* 26, 195 (1976).

References continued

17. L. A. D' Asaro, J.V. Dilorenzo, H. Fuki, *IEEE Trans. Electron. Devices* **ED-25**, 1218 (1978).
18. H. Grebel , B. Iskander, and K.G. Sheppard, *Appl. Phys. Lett.* 55 (25), 2655 (1989).

19. D. R. Turner, *J. Electrochem. Soc.* 107, 810 (1960).

20. D. V. Podlesnik, H. H. Gilgen, R.M. Osgood, and A. Sanchez, *Appl. Phys. Lett.* 43 (12), 1083 (1983).

21. S. Ida and K. Ito, *J. Electrochem. Soc.* 118, 768 (1971).

22. A. E. Williner, D. V. Podlesnik, H. H. Gilgen, R. M. Osgood, *Appl. Phys. Lett.* 53 (13), 1198 (1988).

23. T. Okumura and K. N. Tu, *J. Appl. Phys.* 61 (8), 2955 (1987).

24. Martin von Allmen, Laser-Beam Interactions with Materials, ( Springer-Verlag, New York, 1987):15-20.

25. B. G. Streetman, Solid State Electronic Devices, 3rd. Ed., New Jersey, Prentics-Hall, Inc., (1990): 55-60.

26. S. M. Sze, Semiconductor Devices Physics and Technology , New York, John Wiley & Sons, Inc. , (1985): 61-65, 156-170.

27. G.B. Shinn, F. Steigerwald, H. Stiegler, R. Sauerbrey, F. K. Tittel, and W.L. Wilson, Jr. , Excimer Laser photoablation of silicon, *J. Vac. Sci. Technol.* B, vol. 4, No. 6, 1273 (19860).

28. S. R. Morrison, Electrochemistry at Semiconductor and Oxidized Metal Electrodes , Plenum Press, New York, 1980: 525-527.

29. H. Grebel, B. Iskander, K. G. Sheppard, *J. Appl. Phys.* 67 (4), 1947 (1990).

30. D. S. Boudreaux, F. Williams, A. J. Nozik, *J. Appl. Phys.* 51(4), 2158 (1980).

31. F. Williams and A. J. Nozik, *Nature* 271, 137 (1978).

32. K. D. Moller, Optics, University Service Books, California, (1988): 127-150.

References continued

33. J.W. Goodman, Introduction to Fourier Optics, New York, McGraw-Hill Book Company, (1968): 23-30.

34. H. Grebel and P. Pien, *J. Appl. Phys.* 71 (5), 2428 (1992).

35. S.M. Sze, Physics of Semiconductor Devices , 2nd. ed. , New York, John Wiley & Sons, Inc. , (1981): 243-275.

36. M. O. Aboelfotoh and B. G. Sevensson, *Semiconductor Sci. Tech.* 6 (1991): 647.